

NASA Contractor Report 2998

NASA  
CR  
2998  
c. 1

LOAN COPY - RETURN  
AFWL TECHNICAL LIBRARY  
KIRTLAND AFB, NM

0061659



TECH LIBRARY KAFB, NM

# The Modification and Application of Kuo's Parameterization of Cumulus Convection in Middle Latitudes

Wen-Jey Liang

CONTRACT NAS8-31333  
APRIL 1978

**NASA**





## NASA Contractor Report 2998

# The Modification and Application of Kuo's Parameterization of Cumulus Convection in Middle Latitudes

Wen-Jey Liang  
*University of Oklahoma*  
*Norman, Oklahoma*

Prepared for  
George C. Marshall Space Flight Center  
under Contract NAS8-31333



National Aeronautics  
and Space Administration

**Scientific and Technical  
Information Office**

1978



## TABLE OF CONTENTS

	Page
LIST OF FIGURES. . . . .	iv
LIST OF SYMBOLS. . . . .	vii
Chapter	
I. INTRODUCTION. . . . .	1
II. OBJECTIVE ANALYSIS. . . . .	6
III. VARIATIONAL OPTIMIZATION OF WIND FIELD. . . . .	9
IV. THE MODIFICATIONS OF KUO'S PARAMETERIZATION OF CUMULUS CONVECTION . . . . .	15
V. TESTS . . . . .	28
VI. SUMMARY AND RECOMMENDATIONS . . . . .	40
BIBLIOGRAPHY . . . . .	45
APPENDIX A . . . . .	48
APPENDIX B . . . . .	53
APPENDIX C . . . . .	55
APPENDIX D . . . . .	65

# LIST OF FIGURES

Figure		Page
1.	Grid system. . . . .	69
2.	Synoptic chart for 2100 GMT 11 May 1974 (surface). . . . .	70
3.	Synoptic chart for 2100 GMT 11 May 1974 (850 mb) . . . . .	70
4.	Synoptic chart for 2100 GMT 11 May 1974 (700 mb) . . . . .	71
5.	Synoptic chart for 2100 GMT 11 May 1974 (500 mb) . . . . .	71
6.	Synoptic chart for 2100 GMT 11 May 1974 (400 mb) . . . . .	72
7.	Synoptic chart for 2100 GMT 11 May 1974 (300 mb) . . . . .	72
8.	Synoptic chart for 2100 GMT 11 May 1974 (200 mb) . . . . .	73
9.	Vertical p velocity before optimization at surface. . . . .	73
10.	Vertical p velocity before optimization at 800 mb . . . . .	74
11.	Vertical p velocity before optimization at 700 mb . . . . .	74
12.	Vertical p velocity before optimization at 600 mb . . . . .	75
13.	Vertical p velocity before optimization at 500 mb . . . . .	75
14.	Vertical p velocity before optimization at 400 mb . . . . .	76
15.	Vertical p velocity before optimization at 300 mb . . . . .	76

Figure	Page
16. Vertical p velocity before optimization at 200 mb . . . . .	77
17. Vertical p velocity before optimization at 100 mb . . . . .	77
18. Optimized vertical p velocity at 800 mb. . . .	78
19. Optimized vertical p velocity at 700 mb. . . .	78
20. Optimized vertical p velocity at 600 mb. . . .	79
21. Optimized vertical p velocity at 500 mb. . . .	79
22. Optimized vertical p velocity at 400 mb. . . .	80
23. Optimized vertical p velocity at 300 mb. . . .	80
24. Optimized vertical p velocity at 200 mb. . . .	81
25. Optimized vertical p velocity at 100 mb. . . .	81
26. Horizontal divergence at the test point. . . .	82
27. Vertical p velocity at the test point. . . . .	82
28. Observed temperature and dew-point temperature at the test point. . . . .	83
29. The dry static energy, moist static energy and saturation moist static energy of environment at the test point. . . . .	84
30. The apparent heat source, the apparent moisture sink, and the radiation at the test point . . . . .	84
31. The derived vertical eddy heat flux at the test point . . . . .	85
32. The excess temperature and the excess mixing ratio from the moist adiabat through the lifted condensation level at the test point. . . . .	85
33. Latent heat released computed from large-scale budgets and Kuo's scheme at the test point. . . . .	86

Figure	Page
34. Cumulative mass flux distribution within clouds and the corresponding environmental mass flux computed from the large-scale budgets and Kuo's scheme at the test point . .	86
35. The excess temperature computed from the large-scale budgets and Kuo's scheme at the test point . . . . .	87
36. The excess mixing ratio computed from the large-scale budgets and Kuo's scheme at the test point . . . . .	87
37. Cumulative mass flux distribution within clouds and the corresponding environmental mass flux computed from the large-scale budgets and the modified scheme at the test point . . . . .	88
38. The latent heat released computed from (a) Kuo's scheme, (b) modified scheme and (c) the combination of large-scale budgets and modified scheme at the test point. . . . .	88
39. The excess temperature and the excess mixing ratio from large-scale budgets and modified scheme at the test point. . . . .	89
40. Cumulative mass flux distribution within clouds and the corresponding environmental mass flux from modified scheme at the test point. . . . .	89
41. Three components of the latent heat released computed from modified scheme at the test point. . . . .	90
42. The response function for $\tilde{\alpha} = 0.1$ . . . . .	90

# LIST OF SYMBOLS

$A = \Delta^2 = \Delta x \Delta y$	
$a$	Specified constant
$B$	Production rate of cloudy air
$B_q$	The rate of increase of mixing ratio in a layer in the cloudy region
$b$	The length of the minor axis of an ellipse of constant weight (Chapter II only); the fraction of $M_L$ which is stored in the air to increase the humidity.
$C$	Rate of net condensation in subgrid scale convection
$C_D$	Drag coefficient
$\bar{C}_L$	Condensation rate produced by large-scale motion
$\bar{C}_1$	Condensation rate produced by subgrid-scale motion
$c_p$	Specific heat at constant pressure
$D$	Detrainment
$D_2 = \frac{\partial \bar{v}}{\partial x} + \frac{\partial \bar{u}}{\partial y}$	
$D_1 = \frac{\partial \bar{u}}{\partial x} + \frac{\partial \bar{v}}{\partial y}$	
$E_s$	Rate of evaporation from surface
$e$	Rate of evaporation
$\bar{F}$	Rate of turbulent diffusion of momentum
$g$	Gravitational acceleration
$H_1$	Depth of conditional unstable layer
$H_2$	Height difference between the level where $\theta_e$ is a minimum and the level above where $\theta_e$ is equal to its maximum value below.



$h =$	$C_p T + gz + Lq$
$h^* =$	$C_p T + gz + Lq^*$
$I$	Functional
$K_q$	Horizontal eddy diffusion coefficient for $q$
$K_s$	Horizontal eddy diffusion coefficient for $s$
$K_1$	Critical value of instability (Appendix A only); specified constant
$K_2$	Critical value of low-level convergence (Appendix A only); specified constant
$k$	Specified constant; $\sqrt{m^2+n^2}$ (in Appendix C only)
$\vec{k}$	Unit vector along vertical direction
$k_o$	Karman Constant
$L$	Latent Heat of condensation; differential operator (Appendix C only)
$M_c^*$	The cloud mass flux at the bottom of the detrainment layer
$M_c =$	$-\sigma\omega_c$ , mass flux inside the cloud
$m$	Wave number along $x$ direction
$M_L$	Net convergence of moisture produced by large-scale flow
$M_1$	The amount of moisture needed to create a model cloud over a unit area measured relative to the environment air
$n$	Wave number along $y$ direction
$\vec{n}$	Unit normal vector along the boundary
$P$	Reference pressure
$P_o$	Total precipitation inside the clouds
$p^*$	The level where the surface air becomes saturated by lifting
$p_o$	Mean pressure over the whole region (Appendix C only)

$\Delta p$	$p_s - p_b$ ; the depth of the detrainment layer (Chapter IV only).
$\delta p$	Thickness of a layer
$Q_1 =$	$d\bar{s}/dt$
$Q_2 =$	$-L d\bar{q}/dt$
$Q_c$	Net latent heat released by subgrid scale convection
$Q_R$	Heating rate by radiation
$q$	Mixing ratio of water vapor
$q^*$	Saturated mixing ratio of water vapor
$r$	Distance between the grid point and the observation point
$S_s$	Sensible heat flux from surface
$s =$	$C_p T + gz$
$T$	Temperature
$t$	The time difference from a reference time (Chapter II only); time
$V =$	$ \vec{V} $
$V_{\max}$	The maximum value of the observed wind
$\vec{V} =$	$(u, v)$ , horizontal velocity
$\vec{V}^* =$	$\vec{V} - \tilde{\vec{V}}$ , correction horizontal velocity
$W$	Interpolation weight factor
$W_b$	The weight when $\gamma$ is equal to $b$ and $\theta$ is 90 deg
$x, y$	Horizontal coordinates
$(x_o, y_o)$	The origin of the coordinates on the map
$Y$	The derived vertical eddy heat flux
$z$	Height
$\alpha$	Specified constant

$\tilde{\alpha}$	Relative reliability factor of $\tilde{\omega}$ field
$\beta$	Specified constant
$\gamma =$	$\frac{L}{C_p} \left( \frac{\partial \bar{q}^*}{\partial \bar{T}} \right)_p$
$\Delta$	Grid length
$\nabla$	Horizontal Del operator
$\delta$	Variation
$\epsilon$	Entrainment; small parameter (Appendix C only) .
$\theta$	The angle between the wind direction and the direction from the grid point to the observation point (Chapter II only); potential temperature
$\theta_e$	Equivalent potential temperature
$\Delta \theta_e$	Maximum difference of equivalent potential temperature in conditionally unstable layer
$\lambda_1, \lambda_2$	Lagrange multipliers
$\lambda_b$	A part of $\lambda_1$
$\nu$	Specific constant
$\pi =$	$(P/P_0)^{R/C_p}$
$\rho$	Density
$\sigma$	Fractional area of deep convective systems
$\tau$	Half-life of cloud
$\bar{\tau}$	Period of large-scale flow
$\phi$	The angle between the wind at observation stations and the wind at a grid point; a part of $\lambda_1$ (Appendix C and D only)
$\chi$	Any quantity
$\omega$	$dp/dt$
$\bar{\omega}_m$	Maximum low-level p velocity of large-scale motion
$\omega_t^*$	$\omega_t - \tilde{\omega}_t$ , correction p velocity
$\tilde{\omega}_t$	Vertical p velocity computed from the observed wind and continuity equation

THE MODIFICATION AND APPLICATION OF KUO'S  
PARAMETERIZATION OF CUMULUS CONVECTION  
IN MIDDLE LATITUDES

CHAPTER I

INTRODUCTION

Over many regions in the middle latitudes as well as in the tropics, cumulus convection plays an important role in vertical transport of heat, moisture and horizontal momentum, especially in the warm season (Palmen and Newton, 1969). In these regions, a large portion of the annual precipitation is derived from convective showers and thunderstorms; these storms also account for the greatest weather damage in many areas. Convective systems also are of particular interest because they manifest perhaps the most obvious interaction between disturbances of large and small (or medium) scales. However, because of insufficient resolution of the present observational network, this mechanism must be parameterized in terms of large-scale variables. In the past decade, many parameterizations of cumulus convection have been developed. Each scheme has served surprisingly well in the particular numerical model in which it has been employed. However, because many investigators believe that cumulus convection is a dominant mechanism in the tropics (Riehl and Malkus 1958),

most procedures have been developed for this region. We hardly can expect these schemes to fit our needs in middle latitudes without some modifications.

Currently, two types of cumulus parameterizations are used. One, based on the hypothesis of convective adjustment (Manabe et al., 1965), is utilized in general circulation models and synoptic-scale prediction models. The idea of convective adjustment is based on the assumption that thermal convection develops when the lapse rate of temperature exceeds a certain neutral value. The other, based on the hypothesis of penetrative convection (Ooyama, 1964; Kuo, 1965; Arakawa, 1969), is also utilized in general circulation models; but the scheme is primarily applied to the study of the development of tropical cyclones (Yamasaki, 1968; Ooyama, 1969). Penetrative convection is assumed to occur when cumulus clouds penetrate deeply into an unsaturated atmosphere in areas of low level mass convergence. Although both types of cumulus parameterization have practical significance, the latter appears to be more feasible for our purpose, because the hypothesis of penetrative convection is pertinent for middle-latitude deep convective systems and it can be used to simulate cloud ensembles after some modifications are made. From the simulation of such an ensemble, one can obtain a great deal of information on the statistical properties of the cloud clusters and a deeper understanding of the dynamical mechanisms involved.

Based on the hypothesis of penetrative convection, the parameterization procedure consists of two significant mechanisms involved in the interaction between convection and the environment: 1) adiabatic warming due to the downward motion of the environmental air which compensates for the upward motion inside convective elements, 2) lateral mixing of cloud substance into the environment. Among such parameterization schemes, those developed by Kuo (1965, 1974) and Arakawa (1969, 1974) are two of the most representative. Kuo's scheme is based on a non-steady deep cumulus model; the temperature environment, and the large-scale low-level convergence of moisture are the key indicators. Arakawa's scheme is based on the concept of a balance of the vertical mass transport in the clouds and the environment. Although several authors, such as Ooyama (1971) and Fraedrich (1973, 1974), have developed a theoretical framework to include these mechanisms and to discuss the relationship between these schemes, some confusion still exists (e.g., Ceselski, 1974). It has been stated that Kuo has neglected the heating by adiabatic compression of the slowly descending environment. Also, the reality of the horizontal mixing process involved in his scheme has been questioned. Recently, Kuo (1974) tried to clarify those misunderstandings; however, it is believed that if in Kuo's formulation the terms which account for departures from the area mean, as well as the precipitation terms, are examined carefully, a better explanation can be given.

Kuo's scheme is applicable in those situations where a deep conditionally unstable layer and large-scale low-level convergence are in existence. The former condition makes it possible for huge cumuli to penetrate into the upper troposphere and the lower stratosphere, while the latter condition provides a lifting mechanism to trigger the convective instability. Therefore, in some situations, although the computed fractional area of coverage may be near unity, only shallow or even no clouds may develop. Investigations of moisture convergence and its relationship to severe storm occurrence (e.g., Sasaki 1973) indicate that unstable conditions, downward momentum transport, and other factors, which may be important to thunderstorm outbreaks, are implicitly shown in the moisture convergence patterns. Because we believe that large-scale moisture convergence in a conditionally unstable region is a key mechanism in the development of deep convection, we would like to examine the applicability of Kuo's scheme and to modify it so that the scheme becomes dynamically and practically plausible.

In the following chapters, the AVE II data<sup>1</sup> are utilized to perform the above purposes. In Chapter II, an objective analysis scheme is designed by a best combination of Inman's elliptical weighting function (personal communication) and Barnes' exponential weighting function (Barnes, 1973). In

---

<sup>1</sup>Atmospheric Variability Experiments (AVE) conducted by NASA Marshall Space Flight Center, Huntsville, Alabama.

Chapter III, a variational optimization scheme is developed to ensure accuracy of the divergence and vertical velocity fields. In Chapter IV, Kuo's parameterization scheme is examined and a modified parameterization scheme is proposed and investigated. It is believed that any plausible concepts should be tested by a real situation. Therefore, in Chapter V, a case study is accomplished in order to check the variational optimization scheme, Kuo's parameterization scheme, and the modified parameterization of cumulus convection.



## CHAPTER II

### OBJECTIVE ANALYSIS

In order to compute mass and moisture convergence accurately, a variational optimization scheme has been designed to analyze the wind field. The scheme requires an objective analysis to interpolate values of wind to regularly spaced grid points from the irregularly spaced observation points. The weighting function utilized in the objective analysis should account for the observational resolution and real patterns of the data to avoid any unnecessary errors. Because the large-scale data field is anisotropic and nonhomogeneous, any isotropic or homogeneous weighting function will distort the data field and the unrealistic patterns may occur (McFarland, 1974). In this study, Inman's (1970) elliptic weighting function and Barnes' exponential weighting function (Barnes, 1973) are combined to produce

$$W(r,k) = \exp \left\{ - \frac{\alpha^2 - (\alpha^2 - 1) \cos^2 \theta}{\alpha^2 k^2} r^2 - \frac{t^2}{v} \right\} , \quad (1)$$

where

$$k^2 = - \frac{b^2}{\ln W_b} ,$$

$r$  is the distance between the grid point and the observation point,  $b$  is the length of the minor axis of an ellipse of constant weight,  $\theta$  is the angle between the wind direction

and the direction from the grid point to the observation point,  $W_b$  is the weight when  $r$  is equal to  $b$  and  $\theta$  is 90 deg,  $t$  is the time difference from a reference time,  $v$  is a constant and  $\alpha$  is the ratio of the length of major axis to that of the minor axis  $b$  of an ellipse of constant weight. In this study,  $\alpha$  is chosen as

$$\alpha = a \frac{V}{V_{\max}}, \quad (2)$$

where  $V$  is the wind speed at the observation point,  $V_{\max}$  is the maximum value of the observed wind, and  $a$  is a specified constant.

After the computation of the weighting function from (1) at each grid point, the value of a quantity  $\chi_{ij}$  at the grid point  $(i, j)$  is assigned as

$$\chi_{ij} = \frac{\sum_m W(r_m, k) \chi_m}{\sum_m W(r_m, k)}, \quad (3)$$

where  $\chi_m$  is the value of the quantity  $\chi$  at the  $m$ -th observation point.

In order to better describe the meteorological fields near a frontal zone, the interpolation scheme is utilized twice. In the vicinity of a front, the stations whose winds make a large angle with the wind at a grid point may be separated from the grid point by the front. After the first conventional interpolation, the wind is assigned at each grid point and the angle between the wind at a station and the wind at a grid point can be determined. During the second interpolation, any

stations whose wind make an angle with the wind at a grid point greater than 90 degrees are not utilized in determining the analysis at the grid point. This procedure tends to conserve discontinuities, and is valuable especially near frontal zones.

## CHAPTER III

### VARIATIONAL OPTIMIZATION OF WIND FIELD

In a region of severe convection the vertical velocity is not necessarily zero at an arbitrary level near the cloud tops. However, over a very large region the average vertical velocity should be zero, if  $\frac{\partial P}{\partial t}$  is negligible, to insure conservation of mass. The integral constraint which requires the mean vertical velocity at the top over a large area to be a predetermined value (usually zero) is called the global boundary condition. In this chapter, Sasaki's variational optimization approach is utilized to optimize the entire wind field so that the integrated continuity equation and global boundary condition are satisfied.

In the variational formulation, the upper boundary condition on the vertical velocity at the top of the convective layer should be specified in order to solve the associated Euler-Lagrange equations. However, this condition is unknown. McGinley (1973) assumed that it was zero everywhere. O'Brien (1970) corrected the vertical velocity at the top, which was obtained from the continuity equation and the observed wind field, by the use of the global boundary condition as a strong constraint. However, because the areal mean of the vertical velocity at this level is usually small, the correction is

quite small at most grid points. Furthermore, since the correction is a constant over a horizontal plane (or constant pressure surface), it does not change the vertical velocity patterns. This is desirable only when the vertical velocity patterns obtained from the continuity equation and the observed winds are highly reliable. Indeed, McGinley's top boundary condition is an extreme case of O'Brien's, and is too arbitrary, especially in the vicinity of severe convective systems.

The errors which appear in the vertical velocity field obtained from the continuity equation and the observed wind can be classified as "systematic errors" and "random errors". The systematic errors occur primarily because of inconsistencies between the observed fields and the dynamical model considered. The random errors may be introduced because of inaccuracies of measurements, spatial irregularity of observation points, and by interpolation of values from stations to grid points. Sasaki's variational optimization scheme provides an important advantage by incorporating dynamic, kinematic, statistical and other conditions in data management. Although the random errors can be suppressed by the use of varied filters, the filtering should be incorporated simultaneously in the variational formulation to ensure that the filtered fields satisfy all constraints.

In the following paragraphs, a variational optimization scheme is developed such that systematic errors are suppressed by the use of two strong constraints, i.e., the integrated

continuity equation and the global boundary condition; the random errors are filtered by the use of a low-pass filter. The functional is defined as

$$I = \int_x \int_y \int_p \{ (u - \tilde{u})^2 + (v - \tilde{v})^2 + \tilde{\alpha}^2 (\omega_t - \tilde{\omega}_t)^2 + \tilde{\beta}^2 (\nabla \omega_t \cdot \nabla \omega_t)^2 \} dp dy dx. \quad (4)$$

Here, two strong constraints are utilized:

$$\omega_t = \omega_s - \int_{p_s}^{p_t} \nabla \cdot \tilde{V} dp, \quad (5)$$

$$\int_x \int_y \omega_t dx dy = 0, \quad (6)$$

where  $\tilde{u}$ ,  $u$ ,  $\tilde{v}$ , and  $v$  are observed and optimized wind components along the  $x$  and  $y$  directions, respectively,  $\omega_t$  is the optimized  $p$  velocity at the top of the domain,  $\tilde{\alpha}$  and  $\tilde{\beta}$  are specified parameters,  $p_s$  and  $p_t$  are pressures at the surface and at the top of atmosphere, respectively, and

$$\tilde{\omega}_t = \omega_s - \int_{p_s}^{p_t} \nabla \cdot \tilde{V} dp, \quad (7)$$

$$\omega_s = \tilde{V}_s \cdot \nabla p_s, \quad (8)$$

where  $\tilde{V}_s$  is the observed surface wind and  $\nabla$  is a two dimensional Laplacian differential operator,

$$\nabla \equiv \left( \frac{\partial}{\partial x}, \frac{\partial}{\partial y} \right). \quad (9)$$

After taking the variation of the functional  $I$  and setting it to zero, the associated Euler-Lagrange equations are obtained. These may be written as

$$u = \tilde{u} + \frac{\partial \lambda_1}{\partial x} , \quad (10)$$

$$v = \tilde{v} + \frac{\partial \lambda_1}{\partial y} . \quad (11)$$

$$\tilde{\beta}^2 \nabla^2 \omega_t - \tilde{\alpha}^2 \omega_t + \frac{\lambda_1}{p_s - p_t} = \lambda_2 - \tilde{\alpha}^2 \tilde{\omega}_t , \quad (12)$$

where the associated boundary conditions are

$$\lambda_1 = 0 , \quad (13)$$

and

$$\vec{n} \cdot \nabla \omega_t = 0 , \quad (14)$$

where  $\vec{n}$  is a unit normal vector along the boundary. The derivation of the above equations and the associated boundary conditions are discussed fully in Appendix C.

In order to better understand the physical meaning of this formulation and the associated boundary conditions, let us define the correction velocity,  $\vec{V}^*$ , as

$$\vec{V}^* =: \vec{V} - \tilde{\vec{V}} , \quad (15)$$

where  $\vec{V} = (u, v)$ ,  $\tilde{\vec{V}} = (\tilde{u}, \tilde{v})$ , and  $\vec{V}^* = (u^*, v^*)$ . Substitution of (15) into (4), (10), and (11) leads to

$$I = \int \int \int_{x \ y \ p} \{ \vec{V}^* \cdot \vec{V}^* + \tilde{\alpha}^2 \omega_t^{*2} + \tilde{\beta}^2 (\nabla \omega_t \cdot \nabla \omega_t) \} dp \ dy \ dx , \quad (16)$$

and

$$\vec{V}^* = \nabla \lambda_1 . \quad (17)$$

Eq. (17) shows that the Lagrange multiplier  $\lambda_1$  is the correction velocity potential; i.e., the correction velocity field is irrotational. The first two terms in (4) are the weighted

correction kinetic energy of the region considered, and  $\tilde{\alpha}^2$  is the weighting factor. The third term in (4) is a weak constraint, i.e.,

$$|\nabla \omega_t| \approx 0 \quad (18)$$

Indeed,  $|\nabla \omega_t|$  is a part of the horizontal vorticity associated with  $\omega_t$ . It reflects the spatial distribution of areas of upward and downward motion. In terms of the vertical correction velocity  $\omega_t^*$ , (18) can be written as

$$|\nabla \omega_t^* + \nabla \tilde{\omega}_t| \approx 0 \quad (19)$$

or

$$\left(\frac{\partial \omega_t^*}{\partial x} + \frac{\partial \tilde{\omega}_t}{\partial x}\right)^2 + \left(\frac{\partial \omega_t^*}{\partial y} + \frac{\partial \tilde{\omega}_t}{\partial y}\right)^2 \approx 0 \quad (20)$$

Since the horizontal gradient of the vertical velocity  $\nabla \omega_t$  is zero only when

$$\frac{\partial \omega_t^*}{\partial x} = - \frac{\partial \tilde{\omega}_t}{\partial x} \quad (21)$$

and

$$\frac{\partial \omega_t^*}{\partial y} = - \frac{\partial \tilde{\omega}_t}{\partial y} \quad (22)$$

(19) indicates that (18) is satisfied by introducing a horizontal vorticity  $|\nabla \omega_t^*|$  opposite to the original horizontal vorticity associated with  $\nabla \tilde{\omega}_t$ . Since the horizontal vorticity indicates the spatial distribution of upward and downward motion, any reduction of the horizontal vorticity suppresses the vertical motion. In other words, this procedure smooths



the vertical motion field. The parameter  $\tilde{\beta}$  is selected to accomplish this purpose. In this study, the value of  $\tilde{\beta}$  is assigned to suppress the amplitude of waves whose wave length is less than the distance between adjacent maxima in the large-scale  $\omega$  field.

The boundary condition (13) implies

$$\vec{V}_s^* = \frac{\partial \lambda_1}{\partial s} = 0, \quad (23)$$

along the boundary. Indeed, it is the no-slip boundary condition for the correction velocity field. This condition ensures that the optimization does not change the circulation of the region considered and is consistent with an irrotational correction velocity field. Furthermore, since  $\omega_t$  is unknown, the boundary condition (14) permits  $\omega_t$  to be free on the boundary to allow a wide range of possible  $\omega_t$  patterns.

Eqs. (5), (6), (10), (11), and (12) are five equations for the five unknown,  $u$ ,  $v$ ,  $\omega_t$ ,  $\lambda_1$  and  $\lambda_2$ . Their solutions, derivations and associated response functions are discussed fully in Appendix C. Also, in Appendix D, it is shown that O'Brien's and McGinley's formulations are two special cases of this formulation.

A case study, utilizing NASA AVE II data, is discussed in Chapter V. The results are very encouraging.

## CHAPTER IV

### MODIFICATIONS OF KUO'S PARAMETERIZATION OF CUMULUS CONVECTION

#### A Procedure for Evaluating Cumulus Parameterization Schemes

Described in the following paragraphs is a procedure for examining and evaluating the mechanisms involved in Kuo's (1965) parameterization scheme and in the modified scheme to be specified later. The method is based on the concept that utilization of an accurate expression for the latent heat released by cumulus should lead to good evaluations of other characteristics of the cloud ensemble. It will be shown below that when  $Q_c$ , the latent heat released by cumulus, is expressed in terms of certain cloud ensemble properties, the cloud ensemble properties may be determined from the large-scale budget equations if the time derivatives of dry static energy and mixing ratio in the environment is specified. In other words the cloud ensemble properties computed from this procedure should directly reflect the quality of the expression, for the latent heat released, which is utilized in the parameterization scheme. Furthermore, if the large-scale budgets and the parameterization scheme are both perfect, the latent heat released, as computed from the parameterization scheme

and as determined using the evaluation procedure, should be exactly the same. In the following discussion, any quantity, except the vertical velocity, in the environment is approximated by the area-mean value of that quantity (for more detail, see Appendix A).

First, let us define the dry static energy  $s$  and the moist static energy  $h$  as

$$s \equiv c_p T + gz, \text{ and}$$

$$h \equiv c_p T + gz + Lq,$$

where  $T$  is temperature,  $z$  is height,  $q$  is mixing ratio,  $c_p$  is the specific heat of dry air, and  $g$  is the acceleration of gravity. From (A.2) and (A.3), the heat and moisture equations for the large-scale motion can be written as

$$Q_1 - Q_R \equiv \frac{d\bar{s}}{dt} - Q_R = Q_c + \frac{\partial}{\partial p}[M_c(s_c - \bar{s})], \quad (24)$$

$$- Q_2 \equiv L \frac{d\bar{q}}{dt} = - Q_c + L \frac{\partial}{\partial p}[M_c(q_c - \bar{q})], \quad (25)$$

where  $s_c$ ,  $q_c$ ,  $\bar{s}$  and  $\bar{q}$  are dry static energies and mixing ratios in the cloud and in the environment, respectively,  $Q_R$  is the heating rate by radiation,  $L$  is the latent heat of condensation,  $p$  is pressure,  $Q_c$  is the latent heat released by subgrid scale convection and  $M_c$  is the cloud mass flux defined as  $M_c = -\sigma\omega_c$ , where  $\sigma$  is the fractional area covered by the clouds, and  $\omega_c$  is the pressure velocity inside the clouds.

Also, the saturation moist static energy of the environment,  $\tilde{h}^*$ , is

$$\tilde{h}^* \equiv c_p \bar{T} + g\bar{z} + L\bar{q}^* \equiv \bar{h}^*,$$

where  $\bar{q}^*$  is the saturation mixing ratio at temperature  $\bar{T}$ .

Then, after Arakawa (1969), we have

$$s_c = \bar{s} + \frac{1}{1+\gamma}(h_c - \bar{h}^*) , \quad (26)$$

$$q_c = \bar{q}^* + \frac{\gamma}{(1+\gamma)L}(h_c - \bar{h}^*) , \quad (27)$$

where  $\gamma \equiv \frac{L}{C_p} \left( \frac{\partial \bar{q}^*}{\partial \bar{T}} \right)_p$ .

If  $Q_c$  is expressed in terms of the other variables, combination of (24) - (27) gives four equations for the four unknowns,  $s_c$ ,  $q_c$ ,  $M_c$ , and  $h_c$ . They can be solved provided that the observed large-scale heat and moisture budgets over the area considered are known. The associated boundary conditions are

$$\begin{aligned} \frac{\Delta p}{g}(Q_1 - Q_R) &= S_s - \frac{M_{cb}}{g}(s_{cb} - \bar{s}_b) , \\ - \frac{\Delta p}{g} Q_2 &= LE_s - \frac{M_{cb}}{g} L(q_{cb} - \bar{q}_b) , \\ S_s/LE_s &= C_p(\bar{T}_s - \bar{T}_o)/[L(\bar{q}_s - \bar{q}_o)] , \end{aligned}$$

where the subscript b denotes values at cloud base and  $\bar{T}_s$ ,  $\bar{T}_o$ ,  $\bar{q}_s$ , and  $\bar{q}_o$  are the temperatures and mixing ratios at the surface and at a level above which is representative of the surface boundary layer. Let us define  $Y$  as  $-\overline{\omega' h'}$ . Then, adding (24) and (25) and integrating the resultant equation, we get

$$\begin{aligned} Y(p) &= \int_{p_t}^p (Q_1 - Q_2 - Q_R) dp , \\ &= M_c(h_c - \bar{h}) , \text{ if } p \leq p_b , \end{aligned} \quad (28)$$

where  $p_t$  is the pressure at the top of atmosphere (100 mb in this study);  $Y(p_t)$  is assumed to be zero. Utilizing (28), the boundary conditions are explicitly expressed as

$$M_{cb} = \frac{a_1 - (1+\gamma_b) a_2}{\bar{h}_b^* - \bar{h}_b} , \quad (29)$$

$$h_{cb} = \bar{h}_b + \frac{a_1}{M_{cb}} , \quad (30)$$

where

$$a_1 = g(S_s + LE_s) - \Delta p(Q_1 - Q_R - Q_2) ,$$

$$a_2 = gS_s - \Delta p(Q_1 - Q_R) ,$$

and

$$S_s + LE_s = Y(p_s) ,$$

where  $p_s$  is surface pressure.

#### An Examination of Kuo's Expression for the Release of Latent Heat by Cumulus

In this section, following Kuo (1965),  $Q_c$  is specified as

$$Q_c = B(s_c - \bar{s}) ,$$

which is (A.13) expressed in terms of variables defined in the preceding section. The cloud base is assumed to be at the lifted condensation level representative of the surface layer, and the top of cloud is assumed to be at a level where the temperature of the clouds is equal to that of the environment.

B is expressed according to (32), where  $b$ ,  $M_L$ , and  $M_1$  are defined by (A.12), (A.9), and (A.10), respectively. Substitution of (A.12) and (A.10) into the expression for B leads to

$$B = \frac{1}{M_1} \int_0^{p_s} Q_2 \frac{dp}{g} .$$

Because  $b$  is computed from the local time change of  $\bar{q}$ , from the parameterization point of view  $b$  is unknown and must be specified experimentally. In order to avoid additional error introduced from the specification of values of  $b$ , in this study  $b$  is computed from  $\partial \bar{q} / \partial t$  according to (A.12). The same values of  $b$  are used in the computation of the release of latent heat in the parameterization schemes.

After elimination of  $s_c$ ,  $q_c$  and  $h_c$  from (24) - (27), an ordinary nonlinear differential equation is obtained:

$$\frac{dU}{dp} = F - G/U , \quad (31)$$

where

$$\begin{aligned} U &= M_c \left( \frac{\bar{h} - \bar{h}^*}{1 + \gamma} \right) , \\ F &= Q_1 - Q_R - \frac{B(\bar{h} - \bar{h}^*)}{1 + \gamma} - \frac{\partial}{\partial p} \left( \frac{Y}{1 + \gamma} \right) , \\ G &= \frac{BY}{(1 + \gamma)^2} (\bar{h} - \bar{h}^*) , \text{ and} \\ B &= \frac{M_L}{M_1} (1 - b) , \end{aligned} \quad (32)$$

where  $Y$  is determined from (28) as a function of  $Q_1$ ,  $Q_2$ , and  $Q_R$ , and  $b$  is defined by (A.12).

Eq. (31) can be reduced to Abel's equation of the first

kind and can be solved analytically if the ratio of the two coefficients,  $G$  and  $F$ , is constant, or it can be solved numerically even if the coefficients are variable.  $M_c$  is determined from solutions of (31). Then, according to (28)  $h_c$  can be determined by

$$h_c = \frac{Y}{M_c} + \bar{h}.$$

Next  $s_c$  and  $q_c$  are computed utilizing (26) and (27), respectively, and  $T_c$  is determined by

$$T_c = \frac{s_c - \bar{s}}{C_p} + \bar{T}.$$

Finally,  $Q_c$  may be calculated from (A.13).

Employing the procedures described in the preceding paragraphs, calculations of  $M_c$ ,  $h_c$ ,  $T_c$ ,  $q_c$ ,  $Q_c$ , and heights of cloud tops have been made utilizing NASA AVE II data. Results of these calculations are shown in Figs. 33-36. Although radar charts prepared by the National Weather Service (2035 GMT 11 May 1974) show that the cloud tops were at about 275 mb in the vicinity of the test area, the computed cloud tops are at 556 mb.  $M_c$  computed from (31) is unrealistically large. For example, the values are about an order of magnitude larger than those calculated by Lewis (1975) for a thunderstorm system in central Oklahoma. Also, the latent heat released is about an order of magnitude smaller than required by the large-scale budget equations. All results show that the properties of the cloud ensemble, computed on

the basis of Kuo's expression for the latent heat released, are questionable.

In his tropical prediction model, Krishnamurti (1969) treated the terms which account for departures from the area mean (i.e. vertical diffusion terms) and the precipitation terms, separately. The precipitation terms were computed utilizing an extension of Kuo's scheme, and the vertical diffusion terms were computed utilizing eddy exchange coefficients; the results seem satisfactory. However, other problems still exist. Reed and Recker (1971) found evidence, in a composite Pacific tropical wave, of a heating maximum centered near 400 mb. As mentioned by Ceselski (1974), Kuo's scheme will yield an upper tropospheric heating maximum only if unrealistically deep and hot clouds are assumed. Clouds that include entrainment and extend only to 200 mb or below will generally have maximum  $(T_c - \bar{T})$  in the lower troposphere (Ceselski, 1973). This is particularly true if the disturbance in question is relatively warm in the upper troposphere, as is often the case.

Recently, Edmon and Vincent (1975) have employed Kuo's scheme, as well as the modified scheme by Krishnamurti, to calculate the latent heat released in a case involving the interaction of tropical storm Candy with an intensifying extratropical baroclinic frontal system (0000 - 1200 GMT 25 June 1968). Comparisons between the convective latent heat released and actual precipitation rates show, in general,



that Kuo's scheme and Krishnamurti's scheme fail. They state that there was very little convective latent heat released in the computational region, even though there were widespread thunderstorms during the analysis periods. Therefore, it is necessary to modify Kuo's formulation so that the modified scheme may be applied in middle latitudes.

#### Modified Parameterization of Cumulus convection

Before discussing any modifications, a few statements about the cloud ensemble model proposed in this study are appropriate. Here we assume that the hydro-thermodynamic fluid properties in area  $\sigma$  are the same as those of the environment before the clouds form. Later, clouds form and the whole area  $\sigma$  is covered by clouds, and the hydro-thermodynamic fluid properties in  $\sigma$  are changed from values typical of the environment. During the formation period, entrainment and detrainment, condensation, evaporation, and induced subsidence in the environment may occur. The formation period can be divided into two stages; in the first stage moisture is supplied to the cloud and in the second stage condensation occurs. The conservation law for water vapor implies that there are two sources of water vapor available to produce clouds in a layer. One is the large-scale moisture supply (i.e., the apparent moisture sink) through the lateral boundaries, and the other is vertical moisture convergence inside the cloud across the upper and lower boundaries of the layer. In other words, during the first stage, for the

modified scheme, the rate of increase of mixing ratio in a layer in the cloudy region is formulated as

$$B_q = \frac{Q_2}{L} + \frac{\partial}{\partial p}(M_c q_c) . \quad (33)$$

The second term on the right-hand-side of (33) allows the low level moisture convergence to produce a high level release of latent heat. If (33) is integrated from the top of atmosphere down to the surface, we have

$$\begin{aligned} \frac{1}{g} \int_{p_t}^{p_s} B_q dp &= - \frac{1}{g} \int_{p_t}^{p_s} \frac{\partial \bar{q}}{\partial t} dp - \frac{1}{g} \int_{p_t}^{p_s} \nabla \cdot \bar{q} \vec{V} dp + E_s \\ &= (1 - b) M_L . \end{aligned}$$

The above expression is the same as that used by Kuo to determine the rate at which moisture is supplied to form clouds.

During the condensation stage, a part of the moisture supplied to the cloudy region is utilized to increase the mixing ratio from  $\bar{q}$  to  $q_c$ , and the other part is condensed and latent heat is released. Since the moisture required to produce a unit mass of cloud air (i.e., to increase the mixing ratio and temperature from  $\bar{q}, \bar{T}$  to  $q_c, T_c$ ) in a layer of thickness  $\delta p$  is  $\frac{\delta p}{gL}(h_c - \bar{h})$ , for the modified scheme, the production rate of cloudy air in a layer is expressed as

$$B = \begin{cases} \frac{B_q}{(h_c - \bar{h})/L} & \text{if } B_q > 0 \\ 0 & \text{if } B_q \leq 0 . \end{cases}$$

On the other hand, the conservation law of energy implies that the latent heat released in a layer can be divided into two parts. One part is utilized to heat the air inside the cloud in that layer from  $\bar{T}$  to  $T_c$  and the other part is transported to adjacent layers by the vertical motion in the cloudy region. Therefore, for the modified scheme, the latent heat released is formulated as

$$Q_c = B(s_c - \bar{s}) - \frac{\partial}{\partial p}(M_c s_c) , \quad (34)$$

where  $-\frac{\partial}{\partial p}(M_c s_c)$  is the vertical divergence of dry static energy in the cloudy region. The latent heat released is zero if  $Q_c$  is negative; the level where  $Q_c$  is zero is assumed to be the top of clouds. In other words, the latent heat released is assumed to be zero at the cloud top. If  $M_c$  in (34) is zero, and  $B$  is replaced by  $(1 - b)M_L/M_1$ , (34) is reduced to Kuo's expression for the latent heat released. As shown by Fraedrich (1973), Kuo did not account for the vertical mass flux inside the cloud. Comparison of (34) with (A.13) indicates that a significant modification is that the effect of cloud mass flux on the latent heat released is included in the modified formulation.

A comparison of the modified scheme with the cloud ensemble model proposed by Yanai et al. (1973), may clarify the physical processes allowed in the modified scheme. According to Yanai (1973), if the cloud ensemble is assumed to be in quasi-equilibrium with the large-scale forcing mechanism

(Arakawa and Schubert, 1974), the budget equation for heat inside the clouds may be written as

$$\frac{\partial}{\partial p}(M_c s_c) + \sum_i \epsilon_i \bar{s} - \sum_i D_i s_{ci} + LC = 0, \quad (35)$$

where  $\epsilon_i$ ,  $D_i$  and  $s_{ci}$  are entrainment, detrainment and dry static energy of the  $i$ -th cloud, respectively, and  $C$  is the condensation inside the clouds. Since

$$Q_c = L(C-e), \quad (36)$$

where  $e$  is the rate of evaporation of liquid water detrained from the clouds, combination of (34), (35) and (36) implies

$$B(s_c - \bar{s}) = - \sum_i \epsilon_i \bar{s} + \sum_i D_i s_{ci} - Le. \quad (37)$$

Eq. (37) shows that entrainment, detrainment, and evaporation are parameterized in terms of the temperature difference between the cloud and the environment and the production rate of cloud air. Furthermore, substitution of (34) into (24) leads to

$$Q_1 - Q_R = - M_c \frac{\partial \bar{s}}{\partial p} - \bar{s} \frac{\partial M_c}{\partial p} + B(s_c - \bar{s}).$$

The above equation shows that the apparent heat source for the large-scale motion field, in addition to  $Q_R$ , consists of an adiabatic warming due to downward motion outside the clouds which compensates upward motion (positive  $M_c$ ) inside the clouds, a cooling due to the vertical mass divergence outside the clouds which compensates the vertical mass convergence inside the clouds, and a warming directly due to

the increasing dry static energy inside the clouds.

For the modified parameterization scheme, in order to determine the latent heat released utilizing (34), the cloud mass flux  $M_c$  has to be determined first. A simple two-layer model, which consists of a primary and a detrainment layer, is suggested to accomplish this purpose. Except near the cloud top where a strong detrainment layer exists due to the strong negative buoyancy above the cloud top, the vertical mass convergence inside the cloud in the primary layer is assumed to be proportional to the mass convergence of the large-scale motion and to the fractional increment of moisture inside the clouds; i.e.,

$$\frac{\partial}{\partial p} M_c = \lambda M_c, \text{ where} \quad (38)$$

$$\lambda = -K_1 \nabla \cdot \vec{V} + K_2 \left( \frac{q_c - \bar{q}}{q_c} \right). \quad (39)$$

Indeed, (38) is similar to the conventional entrainment model.

In the detrainment layer near the top of the cloud, the cloud ensemble model is described by the following three equations:

$$0 = -D + \frac{\partial}{\partial p} M_c, \quad (40)$$

$$0 = -Ds_c + \frac{\partial}{\partial p} (s_c M_c) + LC, \quad (41)$$

$$0 = -Dq_c + \frac{\partial}{\partial p} (q_c M_c) - C. \quad (42)$$

The latent heat released is specified as

$$Q_c = -\frac{\partial}{\partial p} (s_c M_c) + D s_c = LC. \quad (43)$$

Eqs. (40), (41), and (42) are similar to those of the cloud ensemble model proposed by Yanai et al. (1973) except that here entrainment is assumed to be negligible compared to detrainment. Eq. (43) shows that production of cloud air is neglected. Evaporation also is neglected because the liquid water content of the clouds is very small at high levels. The solutions of (40), (41), and (42) are

$$\frac{\partial M_c}{\partial p} = D , \quad (44)$$

$$LC = - M_c \frac{\partial}{\partial p} s_c , \text{ and} \quad (45)$$

$$\frac{\partial}{\partial p} h_c = 0 . \quad (46)$$

Eqs. (44), (45), and (46) are three equations for four unknowns,  $T_c$ ,  $M_c$ ,  $C$ , and  $D$ . In this section, one more equation is introduced by assuming that the detrainment,  $D$ , is constant in the layer such that the cloud mass flux  $M_c$  is zero at the top of the clouds; i.e.,

$$D = \frac{M_c^*}{\Delta p} ,$$

where  $\Delta p$  is the depth of the detrainment layer, and  $M_c^*$  is the cloud mass flux at the bottom of the detrainment layer.

In order to make sure that the modified parameterization scheme is reasonable, the procedures described in the first section of this chapter will be utilized; results of this investigation will be discussed in Chapter V. Also, the modified scheme will be compared to Kuo's (1965) scheme.

## CHAPTER V

### TESTS

#### Optimization of the Wind Field

All data are from the second NASA Atmospheric Variability Experiment (AVE II) except for the radiation data. There were fifty-four rawinsonde stations participating in the AVE II Pilot Experiment as shown in Appendix B. Soundings were made at three-hour intervals at each station beginning at 1200 GMT 11 May 1974, and ending at 1200 GMT 12 May 1974. The data were obtained during a period when convective activity was present, large horizontal temperature gradients were evident and rapid changes in weather patterns were occurring. The data area is over the eastern United States east of approximately 105° W longitude. Radar data were obtained from eleven stations located near the center of the observational area, and as much data as possible were collected from the NIMBUS 5, NOAA-3, ATS-3, and DMSP (DAPP) satellites.

The radiation climatological data are from Rodger's results (1967), which are available in the region 0-70 N, 1000-10 mb, and for the months of January, April, July and October. Because the AVE II pilot experiment was held in May, an average of the data for April and July will be utilized in this research.

The synoptic situation of 2100 GMT 11 May 1974 is shown in Figs. 2-8. We choose this particular time because a deep conditionally unstable layer exists over a wide area of the southern United States. There is a cold front across the central part of the country and a warm front extends through the northern states. Three lows and two precipitation areas appear on the map at the analysis time. Also, there is a deep trough in the upper levels extending from north to south across the central United States.

The grid system is shown in Fig. 1; the polar stereographic projection is utilized. The standard latitude and the standard longitude are  $60^{\circ}\text{N}$  and  $100^{\circ}\text{W}$ , respectively. The 11 by 13 computational grid is oriented so that the y-axis is perpendicular to the standard longitude. The map scale is 1:15,000,000, the upper-left-hand corner grid point is located at  $x = 12.6$  in and  $y = 0.97$  in (the origin is at the North pole), and the grid interval is 190.5 km on the image plane.

The interpolation scheme is described in Chapter II. The parameters  $a$ ,  $k$  and  $v$  in (2.2) and (2.1) are  $\sqrt{8}$ , 0.9772, and 2, respectively. During the second interpolation, the weighting function  $W_2$  is assigned as  $W_2 = W_1 \cos \phi$ , where  $\phi$  is the angle between the wind at observation stations and the wind at grid points, and  $W_1$  is the weighting function of the first interpolation determined from (2.1). After interpolation of each variable (i.e., temperature, geopotential height, wind velocity, and mixing ratio) to grid points, mass



divergence and moisture divergence are computed utilizing a fourth-order finite-difference approximation. The vertical  $p$  velocity,  $\omega$ , is determined at each grid point by integration of the continuity equation from the surface; its surface value is determined from (8). Results are shown in Figs. 9-17. The values of  $\omega$  at the surface are very small ( $10^{-5}$  mb sec $^{-1}$ ); the patterns reflect the synoptic situation and orographic lifting. Because of the accumulative errors in the divergence fields, the  $\omega$  fields at higher levels are highly unrealistic, both in pattern and in magnitude. For example, the  $\omega$  patterns don't clearly reveal the areas of upward and downward motion associated with the two troughs in the upper levels, and the magnitudes of the  $\omega$  values are incredibly large, especially at the 100-mb level.

The optimization of the wind field is performed utilizing 0.1 and 0.3, respectively, for the values of the parameters  $\tilde{\alpha}$  and  $\tilde{\beta}$  in (4). Results are shown in Figs. 18 - 25. From 600 mb up to the 100-mb level, the optimized  $\omega$  fields clearly reveal a major trough across the central United States and a minor trough across the southwestern portion of the country. To the east of the major trough, strong upward motion exists and to the west of the major trough strong downward motion is evident in the optimized  $\omega$  fields. Also, there is a small area of upward motion associated with the minor trough in the southwestern United States. All these features were ambiguous before the optimization was accomplished. Also, the

values of  $\omega$  are reduced to reasonable magnitudes by the optimization. Compared to the National Weather Service radar chart for 2035 GMT 11 May 1974, the area of upward motion coincides with the region of deep convection.

### Tests of the Parameterization of Cumulus Convection

In the following paragraphs, Kuo's scheme and the modified scheme are examined by utilizing the procedures discussed in Chapter IV. Eqs. (24) - (27) along with the associated boundary conditions are used in this examination. Since these four equations contain five unknowns,  $s_c$ ,  $q_c$ ,  $h_c$ ,  $M_c$  and  $Q_c$ , an additional equation must be obtained from the formulation of latent heat released. Different formulations of  $Q_c$  provide different solutions. When Kuo's scheme is examined,  $Q_c$  is formulated according to (A.13), and when the modified scheme is investigated,  $Q_c$  is formulated according to (34). The solutions include the latent heat released, the height of the cloud tops, and four bulk properties of the cloud ensemble,  $s_c$ ,  $q_c$ ,  $h_c$  and  $M_c$ . These bulk properties, the latent heat released, and the height of the cloud tops reveal physical insights of the mechanisms involved in each parameterization scheme.

After the evaluation procedure is completed, the latent heat released by cumuli will be determined directly, utilizing both parameterization schemes. The computed latent heat released will be compared to the observations, i.e., to the

precipitation which is required by the large-scale budgets, and to the solutions obtained by utilizing the evaluation procedures specified in Chapter IV.

The tests are performed at grid point (8,9) where a deep unstable layer exists from the lifted condensation level of the surface layer up to the 100-mb level. The horizontal diffusion terms  $\overline{\nabla \cdot \vec{V}'_s}$  and  $\overline{\nabla \cdot \vec{V}'_q}$  in (4.1) and (4.2) are computed by the use of nonlinear horizontal diffusion coefficients similar to those used by Smagorinsky et al. (1965) and Manabe et al. (1965); i.e.,

$$\overline{\nabla \cdot \vec{V}'_s} = \nabla \cdot (K_s \nabla \bar{s}) ,$$

$$\overline{\nabla \cdot \vec{V}'_q} = \nabla \cdot (K_q \nabla \bar{q}) ,$$

$$K_q = K_s = \frac{1}{2} k_o^2 \Delta^2 (D_1^2 + D_2^2)^{1/2} ,$$

where

$$D_1 = \frac{\partial \bar{u}}{\partial x} - \frac{\partial \bar{v}}{\partial y} ,$$

$$D_2 = \frac{\partial \bar{v}}{\partial x} + \frac{\partial \bar{u}}{\partial y} ,$$

$k_o$  is the Karman constant (0.4 in this study), and  $\Delta$  is the grid length. The results show that values of these horizontal diffusion terms are one or two orders of magnitude smaller than those of the apparent heat source,  $Q_1$ , and the apparent moisture sink,  $Q_2$ . The local time changes of the dry static energy and the mixing ratio are determined from observations at 1800 GMT and at 2400 GMT 11 May 1974. Results show that

these two terms are not negligible. The divergence field and the  $\omega$  field are optimized according to the procedures described in Chapter III and in an earlier section of this chapter, and are shown in Figs. 26 and 27. The lifted condensation level is computed according to Inman's approximate formula (1969). The temperature  $\bar{T}$ , the mixing ratio  $\bar{q}$ , the dry static energy  $\bar{s}$ , the moist static energy  $\bar{h}$ , the saturation moist static energy  $\bar{h}^*$ , the apparent heat source  $Q_1$ , the apparent moisture sink  $Q_2$ , the radiation  $Q_R$ , and the derived vertical eddy heat flux  $Y$  are shown in Figs. 28-32. Because of the large horizontal gradients of moisture and temperature in the middle latitudes, the apparent heat source, the apparent moisture sink, and the derived vertical eddy heat flux are about three to five times larger than those of the tropics as determined by Yanai et al. (1973).

In order to obtain a better comparison between the observations and the results computed from the parameterization schemes, the required precipitation is determined from the large-scale heat and moisture budgets as follows. Let us assume that the vertical eddy heat flux and the vertical eddy moisture flux is zero at the cloud tops, i.e.,

$$M_c (s_c - \bar{s})_{p=p_t} = 0 ,$$

$$M_c (q_c - \bar{q})_{p=p_t} = 0 .$$

Then, integration of (24) leads to

$$\frac{1}{g} \int_{p_t}^{p_s} (Q_1 - Q_R) dp = LP_o + S_s, \quad (47)$$

where  $P_o$  is the total precipitation inside the clouds, and  $S_s$  is the rate of transport of sensible heat from the surface. Since the observed tops of clouds are near 275 mb, computations based on the large-scale heat and moisture budgets indicate that the required  $P_o$  is  $0.08 \text{ in hr}^{-1}$ . This amount of precipitation is reasonable compared with observations from the National Weather Service radar charts (2035 GMT 11 May 1974) and Service A teletype reports.

In the evaluation of Kuo's parameterization scheme  $M_c$  is determined from (31) and  $B$  is specified by (32). Because the production rate of cloud air,  $B$ , depends on  $M_c$ , the equations are nonlinear integral-differential equations. A Runge-Kutta method and an iterative technique are utilized to solve the set of equations. The solutions are shown in Figs. 33-36. From these results and (47) the precipitation rate is  $0.00966 \text{ in hr}^{-1}$ , and the cloud top is at 556 mb. Compared to observations, the computed precipitation is one order of magnitude smaller than that observed, and the top of the cloud is about 300 mb lower. Furthermore, the cloud mass flux  $M_c$  and the residual mass flux in the environment,  $\tilde{M}$ , are unrealistically large. These unsatisfactory results may be understood by the following discussion.

Let us rewrite (24) and (25) as follows:

$$Q_c = Q_1 - Q_R - \frac{\partial}{\partial p}[M_c(s_c - \bar{s})] , \quad (48)$$

$$Q_{c/L} = Q_{2/L} + \frac{\partial}{\partial p}[M_c(q_c - \bar{q})] . \quad (49)$$

The first two terms on the right-hand-side of (48) indicate that a part of the latent heat released in a layer is utilized to heat the atmosphere in that layer, and the third term denotes that the other part of the latent heat released is utilized to heat the air in the adjacent layers by means of the vertical motion inside the clouds. The first term on the right-hand-side of (49) indicates that a part of the precipitation in a layer comes from condensation of water vapor in that layer, and the second term shows that the other part of the precipitation comes from the moisture of adjacent layers by means of the vertical motion in the clouds. In other words, latent heat is released as condensation occurs and the dry static energy in a layer is increased. At the same time the vertical eddy flux terms account for the redistribution of moisture and dry static energy. However, because of large horizontal gradients of temperature and moisture in the middle latitudes, the apparent heat source,  $Q_1$ , and the apparent moisture sink,  $Q_2$ , are very large and  $(s_c - \bar{s})$  and  $(q_c - \bar{q})$  are very small. The vertical eddy flux terms may transport the required energy and moisture only when the vertical mass divergence (or convergence) inside the cloud  $\frac{\partial M_c}{\partial p}$ , is extremely

strong. In other words, the cloud mass flux must increase rapidly with height. According to (26) and (28), the cloud temperature can be expressed in terms of  $M_c$ ,  $Y$ , and large-scale variables as

$$T_c = \bar{T} + \frac{1}{C_p(1+\gamma)} \left[ \frac{Y}{M_c} - L(\bar{q}^* - \bar{q}) \right] .$$

From the above equation, it can be seen that as  $M_c$  increases the cloud temperature decreases. When  $M_c$  is sufficiently large that

$$M_c > \frac{L}{Y}(\bar{q}^* - \bar{q}) ,$$

the cloud temperature will be less than that of the environment. In other words, the rapid increase of  $M_c$  with height decreases the cloud temperature and, therefore, suppresses the vertical development of the cloud. This phenomena is verified by the low tops of clouds and the large cloud mass flux in the solutions of the examination of Kuo's scheme. The discussions indicate that a suitable modified scheme should consist of a better mechanism to transport energy and moisture vertically.

The equations and associated boundary conditions utilized in testing the modified parameterization scheme are the same as those used in testing Kuo's scheme except that the latent heat released is formulated according to (34). The equations are nonlinear ordinary differential equations, and a Runge-Kutta method is utilized to solve them. The solutions are shown in Figs. 37-39. From these calculations and (47),

the precipitation rate is  $0.075 \text{ in hr}^{-1}$ , the tops of clouds are at 260 mb, and the maximum latent heat released is at 450 mb. These results agree very well with the observed values.

In order to better explain the improvement of the modified scheme, let us decompose the total latent heat released, as given by (34), into three components as shown below:

$$Q_c = Q_2 \frac{s_c - \bar{s}}{(h_c - \bar{h})} + \frac{L(s_c - \bar{s})}{h_c - \bar{h}} \frac{\partial}{\partial p} (M_c q_c) - \frac{\partial}{\partial p} (s_c M_c) .$$

Each term on the right-hand-side of the above equation is evaluated and the results are plotted in Fig. 41. The first component is due to the large-scale moisture convergence, the second is due to the vertical transport of moisture inside the cloud, and the third represents the vertical divergence of the dry static energy. These three components are nearly equal in magnitude. Therefore, the latent heat released in a layer may not be confined to that layer; the vertical transport of released latent heat is a significant mechanism involved in cumulus convection. Because of the third term, the maximum of the latent heat released is at the 450-mb level. In order to gain insight of the physical meaning of this component, let us consider a special case. If the apparent heat source,  $Q_1$ , is negative such that the rate of increase of moisture in a layer inside the cloud,  $B_q$ , is zero, i.e.,

$$Q_2/L = - \frac{\partial}{\partial p} (M_c q_c) , \quad (50)$$



and (34) becomes

$$Q_c = - \frac{\partial}{\partial p} (M_c s_c) \quad (51)$$

In this situation, although the production rate of cloud air is zero, latent heat is still being released because of the nonzero vertical mass flux inside the clouds. The cloud acts as a machine which pumps the moisture and the dry static energy from the lower levels up to higher levels or vice versa. Also, because the freezing process may occur at the upper levels, the maximum latent heat released may be at the higher levels.

So far, examination of the modified scheme by the use of the large-scale budget equations shows that the modified formulation of latent heat released can better simulate the physical mechanisms involved in the release of latent heat. However, from the parameterization point of view, the cloud mass flux,  $M_c$ , and the cloud temperature have to be determined first in order to utilize the modified scheme to compute the release of latent heat. In this section,  $M_c$  is computed according to (38) and (39). Utilizing 1000 mb as the pressure scale and  $10^{-4} \text{ sec}^{-1}$  as the velocity divergence scale, these two equations can be nondimensionalized, and the dimensionless values of  $K_1$  and  $K_2$  are specified to be 0.18.

Following Kuo, the temperature of the cloud is regarded as the temperature of the moist adiabat through the condensation level representative of the surface layer. Calculations

of  $Q_c$  and  $M_c$  are shown in Figs. 38 and 40. Also, for the modified scheme, the precipitation rate is  $0.0822 \text{ in hr}^{-1}$ , the cloud tops are at 220 mb, and the maximum of the latent heat released is at 400 mb. Compared to the observations, the deviations are only a few percent.

The latent heat released by Kuo's original scheme is shown in Fig. 38. It is about the same amount as accounted for by the first component of the modified formulation. As mentioned by Ceselski (1973) the maximum latent heat released, computed from Kuo's scheme, is often in the lower troposphere; this is verified in Fig. 38.

## CHAPTER VI

### SUMMARY AND RECOMMENDATIONS

The most important feature of the variational optimization scheme developed in this study is that the unknown upper boundary values of the  $\omega$  field become solvable by consideration of the spatial distribution of upward and downward motions. Also, because the functional includes the velocity field and the  $\omega$  field, the procedure insures that both fields are optimized. Each condition and procedure is physically understandable and mathematically rigorous; therefore, the scheme can be assumed to be realistic with a high degree of confidence.

In this study, AVE II data are utilized to verify the reality of the optimization scheme. However, other data sets should also be tested. In order to provide dynamically consistent fields of atmospheric variables as initial conditions in a numerical forecast model utilized to verify the applicability of the modified parameterization scheme, other dynamical and kinematical conditions should be incorporated into the optimization formulation. For example, appropriate advection equations for dry static energy and moisture might be considered.

The most important improvement of the modified para-

meterization scheme is that it models physically realistic processes which may be verified by examination of the large-scale heat and moisture budget equations. Another significant feature is that the modified scheme is consistent with a variable cloud ensemble model which may be time dependent or static, and may or may not account for entrainment, detrainment, and/or evaporation. If large-scale moisture convergence above the cloud base is neglected and cloud mass flux is assumed to be constant with height, the latent heat released in the modified scheme becomes proportional to the cloud mass flux at the cloud base and is similar to that proposed by Ooyama (1969) in his numerical simulation of the life cycle of tropical cyclones. Furthermore, the vertical distribution of the latent heat released, computed from the modified scheme, has a maximum value at the 400-mb level which is physically understandable and is verified by observations (Reed and Recker, 1971). These features are not present in Kuo's scheme.

Although results obtained with the modified scheme are very encouraging, they are still far from perfect. For example, the two-layer model which is utilized to determine the cloud mass flux should be improved. Extensions of this study probably should be focused on the following subjects.

- (a) Improved treatment of evaporative downdraft cooling. This may be the biggest defect of current

versions of all parameterization models. The downdraft cooling is a very effective mechanism to transport the horizontal momentum of upper levels downward and increases the low-level mass convergence around the cloudy area. The low-level mass convergence induced by downdraft cooling can not be observed by the present observational network and should be parameterized in terms of large-scale variables and bulk properties of a cloud ensemble. This may be performed by dividing the cloudy area into downward and upward regions (Asai and Kasahara, 1967); the interaction between these two regions and between cloudy regions and the environment may be revealed by consideration of two sets of cloud ensemble equations. Combination of considerations of downdraft cooling and of the spectral distribution of cloud properties is a very challenging problem for future research.

(b) Improved treatment of the sub-cloud layer. It is evident that accurate determinations of the mass flux, temperature, and moisture content at cloud base are very necessary for accurate computations of latent heat released and of bulk properties of the cloud ensemble. However, because of the poor understanding of atmospheric turbulence, estimates of the flux of heat, momentum, mass, and moisture into the cloud base from the planetary boundary layer are still

highly uncertain. Variational optimization of thermodynamic properties and of the wind field may be utilized to improve the reliability of the computations by employing a planetary boundary layer model. A feasible model should be consistent with the large-scale motion field above the planetary boundary layer such that the derived eddy heat flux,  $Y$ , is nearly zero at the top of atmosphere (or at the tops of the clouds).

(c) Inclusion of the spectral distribution of cloud properties. The clouds may be divided into continuous or discrete categories according to the heights of the cloud tops; it may be assumed that the cloud bases are the same. Since the cloud properties are different for different categories, the latent heat released should be different for different clouds. In order to find the cloud properties and the latent heat released, the spectra of the cloud population should be found first. This may be the key problem for further research.

(d) Improved treatment of radiation term. The radiation term in this study is computed from Rodgers' climatological data. Indeed, clouds can change the radiation dramatically. Some tests show that clouds in an overcast situation change the radiational cooling by one order of magnitude. However, better

radiation results depend on better cloud information, and the cloud information is unknown in the convection-parameterization problem. In order to solve this problem, combination of the parameterization of cumulus convection and a radiation model may be necessary.

(e) Incorporation of scheme into a numerical prediction model. After applying the modified parameterization scheme in a diagnostic sense on several data sets, necessary modifications should be determined in order that the scheme may be incorporated into a regional numerical forecast model such as Kreitzberg's (1974). The scheme should then be inserted into the forecast model and tested on real cases.

## BIBLIOGRAPHY

- Arakawa, A., 1969: Parameterization of cumulus convection. Proc. WMO/IUGG Symp. Numerical Prediction, Tokyo, IV 8, 1-6.
- \_\_\_\_\_, and W. H. Schubert, 1974: Interaction of a cumulus cloud ensemble with the large-scale environment, Part I. J. Atmos. Sci., 31, 674-701.
- Asai, T. and A. Kasahara, 1967: A theoretical study of the compensating downward motions associated with cumulus clouds. J. Atmos. Sci., 24, 487-496.
- Barnes, S. L., 1973: Mesoscale objective map analysis using weighted time-series observations. NOAA Technical Memorandum ERL, NSSL-62.
- Ceselski, B. F., 1973: A comparison of cumulus parameterization techniques. Tellus, 25, 459-478.
- \_\_\_\_\_, 1974: Cumulus convection in weak and strong tropical disturbances. J. Atmos. Sci., 31, 1241-1255.
- Edmore, H. J. and D. G. Vincent, 1975: An application of Kuo's parameterization scheme of convective latent heat release to a middle latitudes cyclone system. Mon. Wea. Rev., (in press).
- Fraedrich, J., 1973: On the parameterization of cumulus convection by lateral mixing and compensating subsidence. Part I. J. Atmos. Sci., 29, 240-243.
- \_\_\_\_\_, 1974: Dynamic and thermodynamic aspects of the parameterization of cumulus convection, Part II. J. Atmos. Sci., 31, 1838-1849.
- Hudson, H. R., 1971: On the relationship between horizontal moisture convergence and convective cloud formation. J. Appl. Meteor., 10, 755-762.
- Inman, R. L., 1969: Computation of temperature at the lifted condensation level. J. Appl. Meteor., 8, 155-158.
- \_\_\_\_\_, 1970: Papers on operational objective analysis schemes at the National Severe Storms Forecast Center. NOAA Technical Memorandum ERLTM-NSSL 51.



- Krishnamurti, T. N., 1969: An experiment in numerical prediction in the equatorial latitudes. Quart. J. Roy. Meteor. Soc., 95, 594-620.
- Kreitzberg, C. W., D. J. Perkey, and J. E. Pinkerton, 1974: Mesoscale modeling and forecasting research. Final report, Dept. of Physics and Atmospheric Science, Drexel University.
- Kuo, H. L., 1965: On the formation and intensification of tropical cyclones through latent heat release by cumulus convection. J. Atmos. Sci., 22, 40-63.
- \_\_\_\_\_, 1974: Further studies of the parameterization of the influence of cumulus convection of large-scale flow. J. Atmos. Sci., 31, 1232-1240.
- Manabe, S., J. Smagorinsky, and R. F. Strickler, 1965: Simulated climatology of a general circulation model with a hydrologic cycle. Mon. Wea. Rev., 93, No. 12, 769-798.
- \_\_\_\_\_: Physical climatology of a general circulation model with a hydrologic cycle. Mon. Wea. Rev., 93, 769-798.
- McFarland, M. J., 1974: Variational optimization analysis of temperature and moisture advection in a severe storm environment. Ph.D. Dissertation, Dept. of Meteor., University of Oklahoma.
- McGinley, J. A., 1973: Environmental energy fields associated with severe storms. M.S. Thesis, Dept. of Meteor., University of Oklahoma.
- Miller, R. C., 1972: Notes on analysis and severe storm forecasting procedures of the air force global weather central. M.A.C. United States Air Force.
- Newman, W. R., 1971: The relationship between horizontal moisture convergence and severe storm occurrences. M.S. Thesis, Dept. of Meteor., University of Oklahoma.
- O'Brien, J. J., 1970: Alternative solutions to the classical vertical velocity problem. J. Appl. Meteor., 9, 197-203.
- Ooyama, K., 1964: A dynamical model for the study of tropical cyclone development. Geofisica Intern. (Mexico), 127-198.
- \_\_\_\_\_, 1969: Numerical simulation of the life cycle of tropical cyclones. J. Atmos. Sci., 26, 3-40.

- \_\_\_\_\_, 1971: A theory on parameterization of cumulus convection, J. Meteor. Soc. Japan, 49, (special issue), 744-756.
- Palmen, E., and C. W. Newton, 1969: Atmospheric Circulation Systems. Academic Press, New York, 391-422.
- Reed, R. J., and E. E. Recker, 1971: Structure and properties of synoptic-scale wave disturbances in the equatorial western Pacific. J. Atmos. Sci., 28, 1117-1133.
- Riehl, H., and J. S. Malkus, 1958: On the heat balance of the equatorial trough zone. Geophysica, 6, 503-538.
- Rodgers, C. D., 1967: The radiative heat budget of the troposphere and lower stratosphere. Report No. A2, Department of Meteorology, Massachusetts Inst. of Technology.
- Sasaki, Y., 1973: Final report of investigation of an operational scheme of analysis and short range prediction of local severe weather. The University of Oklahoma Research Inst.
- Smagorinsky, J., S. Manabe, and J. L. Holloway, 1965: Numerical results from a nine-level general circulation model of the atmosphere. Mon. Wea. Rev., 93, 727-768.
- Yamasaki, M., 1968: Numerical simulation of tropical cyclone development with the use of primitive equations. J. Meteor. Soc. Japan, 46, No. 3, 202-294.
- Yanai, M., 1971: A review of recent studies of tropical meteorology relevant to the planning of GATE. WMO Publ., 2, Annex I, 1-43.
- \_\_\_\_\_, S. Eskensen and J. Chu, 1973: Determination of bulk properties of tropical cloud clusters from large-scale heat and moisture budgets. J. Atmos. Sci., 30, 611-627.

## APPENDIX A

### KUO'S PARAMETERIZATION SCHEME

The large-scale flow variables are interpolated to the grid points of a horizontal grid system with grid length  $\Delta x = \Delta y = \Delta$ . The value of the large-scale flow variable  $\chi_{ij}$  at any grid point can then be taken as representing the average of  $\chi$  over the area  $A = \Delta^2$  centered at this point, while the actual value of  $\chi$  is given by the sum of the average value and the departure, i.e.,

$$\chi = \bar{\chi} + \chi' , \quad \bar{\chi} = \frac{1}{A} \int_A \chi dA , \quad \bar{\chi}' = 0 . \quad (\text{A.1})$$

The grid area  $A$  is chosen to be much larger than the area occupied by a single cumulus cloud and its surrounding descending region such that a large number of clouds are included in  $A$ .

The equations for the potential temperature  $\theta$ , the water vapor mixing ratio  $q$ , and the horizontal velocity  $\vec{V}$  of the large-scale system can be written in  $(x, y, p, t)$  coordinates as shown below. The equation for energy conservation is

$$\frac{d\bar{\theta}}{dt} = Q_R - \frac{L\pi}{C_p} \bar{C}_L = \frac{L\pi}{C_p} \bar{C}_1 - \frac{\partial}{\partial p} \overline{\omega'\theta'} - \nabla \cdot \overline{\vec{V}'\theta'} , \quad (\text{A.2})$$

Also, the equations expressing conservation of moisture and

momentum are

$$\frac{d\bar{q}}{dt} + \bar{C}_L - T_q = -\bar{C}_1 - \frac{\partial}{\partial p} \overline{\omega'q'} - \nabla \cdot \overline{\vec{V}'q'} , \quad (\text{A.3})$$

$$\frac{d\vec{V}}{dt} + f\vec{k} \times \vec{V} + \nabla \phi - \vec{F} = \frac{\overline{\omega'\partial\vec{V}'}}{\partial p} - \overline{\vec{V}' \cdot \nabla \vec{V}'} , \quad (\text{A.4})$$

respectively, where  $\bar{C}_L$  and  $\bar{C}_1$  are the condensation rates produced by the large-scale motions and by the subgrid-scale convective motions, respectively,  $L$  is the latent heat of condensation,  $Q_R$  is the heating rate by radiation and turbulent diffusion,  $T_q$  and  $\vec{F}$  are the rates of turbulence diffusion of moisture and momentum, respectively,  $d/dt$  is  $\partial/\partial t + \vec{V} \cdot \nabla + \omega \frac{\partial}{\partial p}$ , and  $\pi = (P/p)^{R/c_p}$ . The other symbols have their usual meanings.

Assuming that at any given moment the active clouds, including their strongly descending parts, occupy the fractional area  $\sigma$ , while their environments occupy the fractional area  $(1-\sigma)$ , and denoting the flow variables in the active cloud regions by a subscript  $c$  and those in the surrounding regions by a subscript  $d$ , we then have

$$\bar{\chi} = (1-\sigma)\chi_d + \sigma\chi_c , \quad (\text{A.5})$$

where  $\chi$  stands for either  $\omega$ ,  $\vec{V}$ ,  $\theta$ , or  $q$ . Also, by means of algebraic manipulations we obtain

$$\overline{\omega'\chi'} = \frac{\sigma}{1-\sigma} (\omega_c - \bar{\omega})(\chi_c - \bar{\chi}) . \quad (\text{A.6})$$

Since  $\sigma \ll 1$ ,  $\omega_c \gg \bar{\omega}$ , we get

$$\begin{aligned}
\overline{\omega' \chi'} &\doteq - \sigma \omega_c (\bar{\chi} - \chi_c) , \\
&\equiv M_c (\bar{\chi} - \chi_c) \\
&\doteq M_c (\chi_d - \chi_c) , \text{ if } \chi_d \doteq \bar{\chi} .
\end{aligned}
\tag{A.7}$$

Deep cumulus towers and cumulonimbi appear to be associated with a deep conditionally unstable layer and the presence of large-scale convergence (Riehl 1950, Riehl and Malkus 1961). The former of these two conditions make it possible for huge cumuli to penetrate into the upper troposphere and the lower stratosphere, while the latter condition provides a general lifting mechanism to trigger the convective instability. These two conditions can be represented as follows:

$$\begin{aligned}
H_1 H_2 \Delta \bar{\theta}_e &> K_1 \\
- \bar{\tau} \bar{\omega}_m &> K_2 (p_s - p^*)
\end{aligned}
\tag{A.8}$$

where  $\Delta \bar{\theta}_e$  is the maximum difference of the equivalent potential temperature in the conditionally unstable layer,  $H_1$  is the depth of this layer,  $H_2$  the height difference between the level where  $\theta_e$  is a minimum and the level above when  $\theta_e$  is equal to its maximum value below,  $\bar{\tau}$  is the period of the large-scale flow,  $p_s - p^*$  is the lift needed for the surface air at the level  $p_s$  to become saturated,  $\bar{\omega}_m$  the maximum low-level p-velocity, and  $K_1$  and  $K_2$  are critical values of instability and low-level convergence, respectively, which ensure that deep convergence will develop. Kuo used the net convergence of moisture into the vertical column of air of unit cross

section produced by the large-scale flow and by evaporation from the ground as one fundamental parameter. Let this quantity be  $M_L$ ; then,

$$M_L = - \frac{1}{g} \int_0^{p^*} (\nabla \cdot \bar{\vec{V}}_q) dp + \bar{\zeta}_o C_D \bar{V}_o (\bar{q}_s - \bar{q}_o) , \quad (A.9)$$

where subscripts s and o indicate values at the surface and at a nearby higher level, respectively, and  $C_D$  is the drag coefficient.

The amount of moisture needed to create a deep cumulus of area  $\sigma$  and pressure depth  $p_b - p_t$  with temperature  $T_c$  and saturation mixing ratio  $q_c(T_c)$  is

$$\sigma M_1 = \frac{\sigma}{g} \int_{p_t}^{p_b} \left[ \frac{C_p}{L} (T_c - \bar{T}) + (q_c - \bar{q}) \right] dp . \quad (A.10)$$

This is supplied by the large-scale convergence of moisture in time  $\tau$ . Hence,

$$\sigma = \frac{\tau M_L}{M_1} , \quad (A.11)$$

where  $\tau$  is the half-life of the cloud (approximately 30 minutes).

Let's assume that a fraction  $(1-b)$  of the total convergence of moisture  $M_L$  is condensed and either precipitated out as rain or was carried away, while the remaining fraction  $b$  of  $M_L$  is stored in the air to increase the humidity (including the influence of evaporation of condensed water). That is to say, we have

$$b M_L = \frac{1}{g} \int_0^{p_o} \frac{\partial \bar{q}}{\partial t} dp . \quad (A.12)$$

Now, according to Kuo (1965), the rate of the release of latent heat  $Q_c$  is

$$Q_c = \frac{\sigma}{\tau} C_p (T_c - \bar{T}) (1 - b) \quad (\text{A.13})$$

Also, according to Kuo (1974), the vertical velocity  $\omega_c$  is approximated as

$$\omega_c = - \frac{\theta_c - \bar{\theta}}{\tau (\partial \theta_e / \partial p)_{ef}} \quad (\text{A.14})$$

where  $(\partial \theta_e / \partial p)_{ef} = \partial \bar{\theta} / \partial p + \frac{L}{C_p} (\partial q_c / \partial p)$ .

Kuo suggested that the temperature  $T_c$  of the cloud can be taken as the temperature  $T_{es}$  of the moist adiabat through the condensation level of the representative surface air, as a first approximation.

## APPENDIX B

### RAWINSONDE STATIONS FOR AVE II PILOT EXPERIMENT

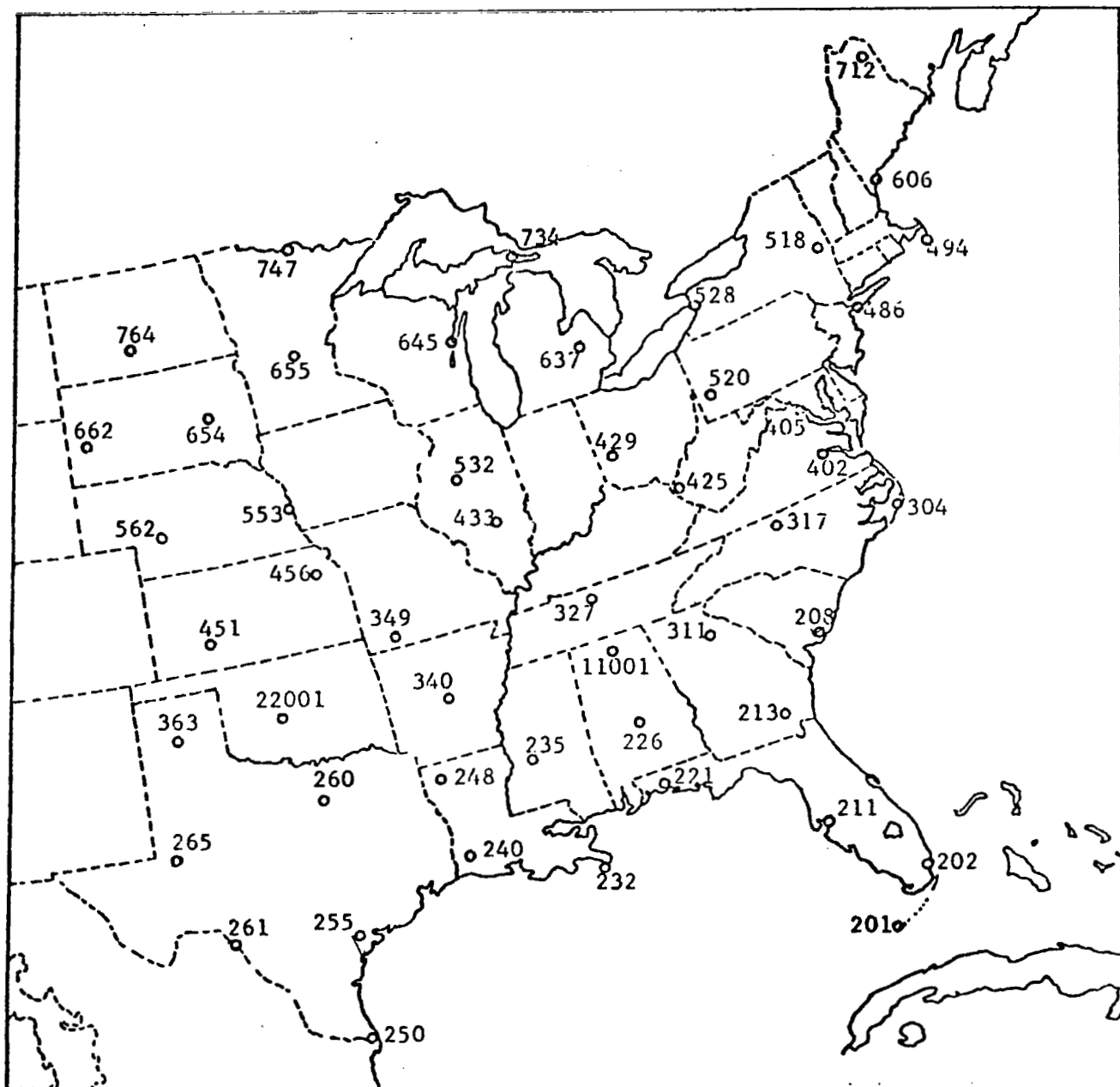


Fig. B.1. Rawinsonde stations for AVE II Pilot Experiment.



Table B.1

## List of Rawinsonde Stations for AVE II Pilot Experiment

<u>Station Number</u>	<u>Location</u>
11001 (MSF)	Marshall Space Flight Center, Alabama
22001 (OUN)	Norman, Oklahoma
22002 (FSI)	Ft. Sill, Oklahoma
22003 (LNS)	Lindsay, Oklahoma
22004 (FTC)	St. Cobb, Oklahoma
22005 (CHK)	Chickasha, Oklahoma
201 (EYW)	Key West, Florida
202 (MIA)	Miami, Florida
208 (CHS)	Charleston, South Carolina
211 (TPA)	Tampa, Florida
213 (AYS)	Waycross, Georgia
221 (VPS)	Eglin AFB, Florida
226 (MGM)	Montgomery, Alabama
232 (BVE)	Boothville, Louisiana
235 (JAN)	Jackson, Mississippi
240 (LCH)	Lake Charles, Louisiana
248 (SHV)	Shreveport, Louisiana
250 (BRO)	Brownsville, Texas
255 (VCT)	Victoria, Texas
260 (SEP)	Stephenville, Texas
261 (DRT)	Del Rio, Texas
265 (MAF)	Midland, Texas
304 (HAT)	Hatteras, North Carolina
311 (AHN)	Athens, Georgia
317 (GSO)	Greensboro, North Carolina
327 (BNA)	Nashville, Tennessee
340 (LIT)	Little Rock, Arkansas
349 (UMN)	Monette, Missouri
363 (AMA)	Amarillo, Texas
402 (WAL)	Wallops Island, Virginia
405 (IAD)	Dulles Airport, Virginia
425 (HTS)	Huntington, West Virginia
429 (DAY)	Dayton, Ohio
433 (SLO)	Salem, Illinois
451 (DOC)	Dodge City, Kansas
456 (TOP)	Topeka, Kansas
486 (JFK)	Kennedy Airport, New York
494 (CHH)	Chatam, Massachusetts
518 (ALB)	Albany, New York
520 (PIT)	Pittsburg, Pennsylvania
528 (BUF)	Buffalo, New York
532 (PIA)	Peoria, Illinois
553 (OMA)	Omaha, Nebraska
562 (LBF)	North Platte, Nebraska
606 (PWM)	Portland, Maine
637 (FNT)	Flint, Michigan
645 (GRB)	Green Bay, Wisconsin
654 (HUR)	Huron, South Dakota
655 (STC)	St. Cloud, Minnesota
662 (RAP)	Rapid City, South Dakota
712 (CAR)	Caribou, Maine
734 (SSM)	Sault Ste Marie, Michigan
747 (INL)	International Falls, Minnesota
764 (BIS)	Bismarck, North Dakota

## APPENDIX C

### SOLUTIONS OF $(\lambda_1, \lambda_2)$ EQUATION SET AND THEIR RESPONSE FUNCTIONS

As shown in Chapter III, the functional is defined as

$$I = \int \int \int_{x \ y \ p} [(u-\tilde{u})^2 + (v-\tilde{v})^2 + \tilde{\alpha}^2 (\omega_t - \tilde{\omega}_t)^2 + \tilde{\beta}^2 (\nabla \omega_t \cdot \nabla \omega_t)] dp \ dy \ dx, \quad (C.1)$$

and is associated with two strong constraints:

$$\omega_t = \omega_s - \int_{p_s}^{p_t} \nabla \cdot \vec{v} \ dp, \quad (C.2)$$

$$\int \int_{x \ y} \omega_t \ dx \ dy = 0, \quad (C.3)$$

where each symbol is defined in Chapter III.

Let us take the variation of the functional  $I$  and set it to zero, i.e.,

$$\begin{aligned} \delta I = & 2 \int \int \int_{x \ y \ p} \left\{ [(u-\tilde{u}) - \frac{\partial \lambda_1}{\partial x}] \delta u + [(v-\tilde{v}) - \frac{\partial \lambda_1}{\partial y}] \delta v + [\tilde{\alpha}^2 (\omega_t - \tilde{\omega}_t) + \right. \\ & + \frac{\lambda_1}{p_t - p_s} + \lambda_2 - \tilde{\beta}^2 \nabla^2 \omega_t] \delta \omega_t \Big\} dp \ dy \ dx + \int \int_{y \ p} [\lambda_1 \delta u]_{x=x_1}^{x=x_2} dp \ dy \\ & + \int \int_{x \ p} [\lambda_1 \delta v]_{y=y_1}^{y=y_2} dp \ dx + \int \int_{y \ p} [\tilde{\beta}^2 \frac{\partial \omega_t}{\partial x}]_{x=x_1}^{x=x_2} dp \ dy + \\ & + \int \int_{x \ p} [\tilde{\beta}^2 \frac{\partial \omega_t}{\partial y}]_{y=y_1}^{y=y_2} dp \ dx = 0, \end{aligned} \quad (C.4)$$

where  $x_1$  and  $x_2$  are the boundary values of  $x$  corresponding to the value of  $y$  and  $p$  held constant in the  $x$ -integration,  $y_1$  and

$y_2$  are the boundary values of  $y$  corresponding to the value of  $x$  and  $p$  held constant in the  $y$ -integration, and  $\nabla^2$  is a two dimensional Laplacian operator. Then, the associated Euler-Lagrange equations are:

$$u = \tilde{u} + \frac{\partial \lambda_1}{\partial x} , \quad (C.5)$$

$$v = \tilde{v} + \frac{\partial \lambda_1}{\partial y} , \quad (C.6)$$

$$\beta^2 \nabla^2 \omega_t - \tilde{\alpha}^2 \omega_t + \frac{\lambda_1}{p_s - p_t} = \lambda_2 - \tilde{\alpha}^2 \tilde{\omega}_t . \quad (C.7)$$

For the elimination of the last four terms in (C.4), there are several choices of boundary conditions associated with Lagrange multiplier  $\lambda_1$ , the derivatives of  $\omega_t$ , and the variations of  $u$ ,  $v$ , and  $\omega_t$ . In this study, the associated boundary conditions are:

$$\lambda_1 = 0 , \quad (C.8)$$

$$\vec{n} \cdot \nabla \omega_t = 0 , \quad (C.9)$$

where  $\vec{n}$  is an unit normal vector along the boundary. The physical explanations of the variational formulation and the associated boundary conditions are presented in Chapter III.

Eqs. (C.2), (C.3), (C.5), (C.6), and (C.7) are five equations for five unknowns:  $u$ ,  $v$ ,  $\omega_t$ ,  $\lambda_1$ , and  $\lambda_2$ . Substituting (C.5) and (C.6) into (C.2), we get

$$\omega_t = \tilde{\omega}_t + (p_s - p_t) \nabla^2 \lambda_1 . \quad (C.10)$$

The substitution of (C.10) into (C.7) leads

$$\tilde{\beta}^2 \nabla^2 [(p_s - p_t) \nabla^2 \lambda_1] - \tilde{\alpha}^2 (p_s - p_t) \nabla^2 \lambda_1 + \frac{\lambda_1}{p_s - p_t} = \lambda_2 - \tilde{\beta}^2 \nabla^2 \tilde{\omega}_t \quad (\text{C.11})$$

From Gauss' theorem and the boundary condition (C.9), we have

$$\begin{aligned} \nabla^2 \omega_t &\equiv \frac{\int \int_{x,y} (\nabla^2 \omega_t) dx dy}{\int \int_{x,y} dx dy} \\ &= \frac{\int_C (n \cdot \nabla \omega_t) ds}{\int \int_{x,y} dx dy} \\ &= 0, \end{aligned}$$

where C is the boundary of the area considered, and  $(\bar{\phantom{x}})$  is an area-average operator. After applying the area-average operator to (C.7), we get

$$\lambda_2 = \tilde{\alpha}^2 \bar{\tilde{\omega}_t} + \overline{\left( \frac{\lambda_1}{p_s - p_t} \right)}, \quad (\text{C.12})$$

where the strong constraint (C.3) has been utilized.

Eqs. (C.11) and (C.12) contain two unknowns:  $\lambda_1$  and  $\lambda_2$ . Solutions can be obtained by an iterative technique. Fortunately, because the equations are linear and  $\lambda_2$  is constant, the solutions can be determined without using an iterative procedure. In order to clarify the procedures utilized to obtain solutions, let us define a linear differential operator L as:

$$L \equiv \tilde{\beta}^2 \nabla^2 (p_s - p_t) \nabla^2 - \tilde{\alpha}^2 (p_s - p_t) \nabla^2 + \frac{1}{p_s - p_t}.$$

Then, (C.11) can be rewritten as

$$\lambda_1 = L^{-1} (\lambda_2 - \tilde{\beta}^2 \nabla^2 \tilde{\omega}_t). \quad (\text{C.13})$$

where  $L^{-1}$  is the inverse operator of  $L$ .

Setting

$$\lambda_1 = \lambda_b + \phi , \quad (C.14)$$

where

$$\lambda_b = L^{-1}(-\tilde{\beta}^2 \nabla^2 \tilde{\omega}_t) \quad (C.15)$$

and the boundary values of  $\lambda_b$  and  $\phi$  are chosen to be zero, then, (C.13) and (C.12) become

$$\phi = L^{-1}(\lambda_2) , \quad (C.16)$$

$$\lambda_2 = C + \overline{\left(\frac{\phi}{p_s - p_t}\right)} , \quad (C.17)$$

where

$$C = \tilde{\alpha}^2 \overline{\tilde{\omega}_t} + \left(\frac{\lambda_b}{p_s - p_t}\right) .$$

From (C.15),  $\lambda_b$  can be solved by using a relaxation method. After  $\phi$  and  $\lambda_2$  are determined from (C.16) and (C.17), the complete solution is obtained from (C.14). Eqs. (C.15) and (C.16) show that  $\lambda_b$  is a part of the solution of  $\lambda_1$  which corresponds to the curvature of the  $\tilde{\omega}_t$ -field, and  $\phi$  is the other part of the solution of  $\lambda_1$  which corresponds to the mean value of  $\tilde{\omega}_t$ . These properties will be discussed in detail later.

In order to employ iterative procedures to solve for  $\phi$  and  $\lambda_2$ , let us rewrite (C.16) and (C.17) as

$$\phi^{(k)} = L^{-1}(\lambda^{(k)}) , \quad (C.18)$$

$$\lambda_2^{(k)} = C + \frac{\phi^{(k-1)}}{p_s - p_t}, \quad (C.19)$$

where  $(k)$  indicates the  $k$ -th iteration. Let zero be the first guess for the solution of  $\phi$ , and define

$$\frac{\overline{L^{-1}(C)}}{p_s - p_t} \equiv aC,$$

i.e.,

$$a \equiv \frac{\overline{L^{-1}(C)}}{p_s - p_t} \cdot \frac{1}{C}.$$

Then, (3.21) and (3.22) become

$$\lambda^{(n)} = C \sum_{k=0}^n a^k, \quad (C.20)$$

$$\phi^{(n)} = \phi^{(0)} \sum_{k=0}^n a^k, \quad (C.21)$$

and

$$\phi^{(0)} \equiv L^{-1}(C). \quad (C.22)$$

The derivation of (C.20) and (C.21) are mainly based on the facts that the operator  $L$  is linear and  $\lambda_2$  is constant. It is obvious that if  $|a| < 1$ , the iteration procedure is convergent provided  $C$  and  $\phi^{(0)}$  are bounded. Since  $a$  is a function of  $\tilde{\alpha}$  and  $\tilde{\beta}$ , a diagram, as shown in Fig. C.1, can be constructed to determine the convergent and divergent region in  $(\tilde{\alpha}, \tilde{\beta})$  space. Convergence of the iterative procedure has been investigated for several cases. If the variables are nondimensionalized by suitable scales (e.g. the scale for the vertical  $p$  velocity

should be  $10^{-3} \text{ mb sec}^{-1}$ , and the mass convergence scale should be  $10^{-5} \text{ sec}^{-1}$ , etc.), all tested cases show that the iteration procedure is convergent (rapidly in most cases) for a wide range of values of  $\tilde{\alpha}$  and  $\tilde{\beta}$ .

In the convergence region, the solution of (C.20) and (C.21) is

$$\begin{aligned}\lambda_2 &= \lambda_2^{(\infty)} = \frac{d}{1-a} , \\ \phi &= \phi^{(\infty)} = \frac{\phi^{(0)}}{1-a} ,\end{aligned}\tag{C.23}$$

and the complete solution of (C.11) and (C.12) is obtained by use of (C.14).

Following the same concepts utilized in obtaining solutions to (C.14),  $\omega_t$  is written as

$$\omega_t = \omega_t^b + \omega_t^\phi \tag{C.24}$$

where  $\omega_t^b$  corresponds to  $\lambda_b$  and  $\omega_t^\phi$  corresponds to  $\phi$ . Referring to (C.10),  $\omega_t^b$  and  $\omega_t^\phi$  may be chosen as

$$\omega_t^b = \tilde{\omega}_t + (p_s - p_t) \nabla^2 \lambda_b , \tag{C.25}$$

$$\omega_t^\phi = (p_s - p_t) \nabla^2 \phi , \tag{C.26}$$

and the associated boundary conditions are

$$\vec{n} \cdot \nabla \omega_t^b = \vec{n} \cdot \nabla \omega_t^\phi = 0 . \tag{C.27}$$

Boundary conditions different from (C.27) may be posed, although we prefer (C.27) because they are simple and are consistent with (C.9). According to (C.25) and (C.26),  $\omega_t^b$

and  $\omega_t^\phi$  can be determined from  $\lambda_b$  and  $\phi$ , and then  $\omega_t$  can be obtained from (C.24).

Figs. 9-26 provide examples of this optimization scheme. Comparisons of these vertical velocity fields before and after optimization are discussed fully in Chapter V.

In order to better understand how to choose suitable values for  $\tilde{\alpha}$  and  $\tilde{\beta}$ , the associated response function has to be found. Let us assume that

$$p_s - p_t = p_o + p' ,$$

$$p' = \sum_{k=1}^{\infty} \epsilon p_k ,$$

where  $\epsilon$  is a small parameter,  $p_o$  is the mean value over the whole region, and  $p'$  is the fluctuation of  $(p_s - p_t)$  from  $p_o$ . Since the ratio of  $p'$  to  $p_o$  is smaller than 0.1 and is less than 0.02 at most grid points,  $p'$  is treated as a small perturbation. The differential operator  $L$  can be expanded as:

$$L = (\tilde{\beta}^2 p_o \nabla^4 - \tilde{\alpha}^2 p_o \nabla^2 + \frac{1}{p_o}) + \{ \tilde{\beta}^2 \nabla^2 p' \nabla^2 - \tilde{\alpha}^2 p' \nabla^2 + \frac{1}{p_o} \sum_{k=0}^{\infty} (-\frac{p'}{p_o})^k \} = L_o + O(\epsilon) ,$$

where

$$L_o \equiv \tilde{\beta}^2 p_o \nabla^4 - \tilde{\alpha}^2 \nabla^2 + \frac{1}{p_o} ,$$

and  $O(\epsilon)$  indicates the order of magnitude of  $\epsilon$  (less than 0.1 in this study). To the zeroth order approximation, (C.15) and (C.16) become



$$\lambda_b = L_o (-\tilde{\beta}^2 \nabla^2 \tilde{\omega}_t) \quad (C.28)$$

$$\phi = L_o (\lambda_2) .$$

The solution of  $\phi$  is simply

$$\phi = p_o \lambda_2 . \quad (C.29)$$

From Fourier transformation (FT) theory, any function  $\lambda(x,y)$  and its Fourier transform  $C(m,n)$  are represented as

$$\lambda(x,y) = FT^{-1}(C(m,n)) = \sum_{n=-\infty}^{\infty} \sum_{m=-\infty}^{\infty} C(m,n) e^{i(mx+ny)} dm dn , \quad (C.30)$$

$$C(m,n) = FT(\lambda(x,y)) = \frac{1}{L_x L_y} \int_{-\frac{L_y}{2}}^{\frac{L_y}{2}} \int_{-\frac{L_x}{2}}^{\frac{L_x}{2}} \lambda(x,y) e^{-i(mx+ny)} dx dy , \quad (C.31)$$

where  $m$ ,  $L_x$ ,  $n$  and  $L_y$  are the wave numbers and the width of the domain along the direction of  $x$  and  $y$ , respectively.

Utilizing (C.30) and (C.31), (C.28) becomes

$$\begin{aligned} \gamma^b &\equiv \frac{C^b(m,n)}{\tilde{C}_w(m,n)} \\ &= \frac{\tilde{\beta}^2 k^2}{(\tilde{\beta}^2 k^2 + \tilde{\alpha}^2) k^2 p_o + \frac{1}{p_o}} , \end{aligned}$$

where  $k^2 = m^2 + n^2$ ,

$C^b(m,n)$  is the Fourier transform of  $\lambda_b$ , and  $\tilde{C}_w(m,n)$  is the Fourier transform of  $\tilde{\omega}_t$ . Similarly, from (C.25), we have

$$\alpha_w^b \equiv \frac{C_w^b(m,n)}{\tilde{C}_w(m,n)}$$

$$= 1 - \frac{p_o \tilde{\beta}^2 k^4}{(\tilde{\beta}^2 k^2 + \tilde{\alpha}^2) k^2 p_o + \frac{1}{p_o}} ,$$

where  $C_w^b(m,n)$  is the Fourier transform of  $\omega_t^b$ , and  $C_w^\phi(m,n)$  is the Fourier transform of  $\omega_t^\phi$ .

In spite of the value of  $\tilde{\alpha}$ ,  $\alpha_w^b$  approaches 1 and  $\gamma^b$  approaches zero as  $\tilde{\beta}$  approaches zero for any  $m$ , and  $n$ . It implies that  $C_w^b(m,n)$  approaches  $\tilde{C}_w(m,n)$  and  $\lambda_b$  approaches zero, i.e., no filtering of the  $\omega_t^b$  field. It is always true even if  $p'$  is not negligibly small. On the other hand, as  $\tilde{\beta}$  becomes very large, we have

$$\gamma^b \sim \frac{1}{p_o k^2} ,$$

and

$$\gamma_w^b \sim 0 .$$

The above equations show that the values of  $\gamma_b$  are dominated by long waves as  $\tilde{\beta}$  becomes large. It also implies that  $\omega_t^b$  approaches zero as  $\tilde{\beta}$  approaches infinity.

Since  $\lambda_2$  is a constant, the combination of (C.29) and (C.26) implies

$$\omega_t^\phi = 0 ,$$

identically. The above equation indicates that when  $p'$  is small, most of the adjustment of the vertical velocity (or mass convergence) is due to the  $\omega_t^b$  part. It will be shown, in

Appendix D, that when  $\tilde{\beta}$  is zero, the adjustment is very small, provided a reasonable value of  $\tilde{\alpha}$  (e.g.,  $\tilde{\alpha} = 0.1$ ) is utilized.

According to the above discussion, several numerical examples of the response function are shown in Fig. 42. Generally speaking, for synoptic-scale systems, errors in the velocity field are of the order of 10 percent and errors in the  $\omega$  field may be ten times larger. In other words, the reliability of the velocity field may be ten times larger than that of the  $\omega$  field, and, therefore,  $\tilde{\alpha}$  may be chosen as 0.1 in the optimization scheme. Since the wavelength of resolvable waves is about 600 km and the width of the area considered is about 2000 km, waves whose wave number is less than three should be suppressed. Also, for the synoptic situation under study, the distance between adjacent extrema in the vertical motion field is between 700 and 1000 km. Therefore, the most important waves are those of wave number one or two. Values of  $\tilde{\beta}$  between 0.1 and 0.3 should be very good in this situation.

## APPENDIX D

### SOME SPECIAL CASES OF THE VARIATIONAL OPTIMIZATION SCHEME

If  $\tilde{\beta}$  is zero, (C.17) becomes

$$\nabla^2 \lambda_b - \frac{\lambda_b}{\tilde{\alpha}^2 (p_s - p_t)^2} = 0 . \quad (D.1)$$

Since  $\tilde{\alpha}^2$  and  $(p_s - p_t)^2$  are both positive, the solution of (D.1) may be expressed in terms of the Green's function,  $G(x, y, \zeta, \eta)$  as

$$\lambda_b(x, y) = \int_C \lambda_b(x, y, \zeta, \eta) \frac{\partial G(x, y, \zeta, \eta)}{\partial n} ds ,$$

where  $n$  and  $s$  are the coordinates perpendicular and tangential to the boundary  $C$ , respectively. Because  $\lambda_b$  is zero along the boundary, the solution of (D.1) is simply

$$\lambda_b = 0 , \quad (D.2)$$

identically. As  $\tilde{\alpha}$  approaches zero, (C.18) and (C.10) become

$$\lambda_1 = \phi = \lambda_2 (p_s - p_t) \quad (D.3)$$

and

$$\omega_t = \tilde{\omega}_t + (p_s - p_t) \lambda_2 \nabla^2 (p_s - p_t) . \quad (D.4)$$

Substituting (D.4) into (C.3), we get

$$\lambda_2 = - \frac{\tilde{\omega}_t}{[(p_s - p_t) \nabla^2 (p_s - p_t)]} \quad (D.5)$$

(D.3), (D.4) and (D.5) imply that if  $(p_s - p_t)$  is a constant,  $\omega_t$  is equal to  $\tilde{\omega}_t$ . In this case, the adjustment of  $\tilde{\omega}_t$  is impossible. In other words, the horizontal curvature of the  $(p_s - p_t)$  field is the only mechanism to adjust the observation field such that the continuity equation and the global upper boundary condition of vertical p-velocity are satisfied.

If  $\beta$  is zero and  $\tilde{\alpha}$  approaches infinity,  $\lambda_b$  is zero identically, and (C.18) and (C.10) may be written as

$$\nabla^2 \lambda_1 = - \frac{\lambda_2}{(p_s - p_t)} \quad (D.6)$$

$$\omega_t = \tilde{\omega}_t - \lambda_2 .$$

The above two equations imply

$$\lambda_2 = \overline{\tilde{\omega}_t} . \quad (D.7)$$

Since

$$\omega = \omega_s - \int_{p_s}^p \nabla \cdot \vec{V} \, dp ,$$

and

$$\tilde{\omega} = \omega_s - \int_{p_s}^p \nabla \cdot \vec{V} \, dp ,$$

we have

$$\begin{aligned} \omega - \tilde{\omega} &= - \int_{p_s}^p (\nabla \cdot \vec{V} - \nabla \cdot \vec{\tilde{V}}) \, dp \\ &= - \int_{p_s}^p \nabla^2 \lambda_1 \, dp \\ &= - \left( \frac{p_s - p}{p_s - p_t} \right) \overline{\tilde{\omega}_t} . \end{aligned} \quad (D.8)$$

(D.8) is the differential form of O'Brien's formulation (1970). Because the correction velocity field is irrotational, the optimized wind field can be determined after the correction velocity potential is determined from (D.6) and (D.7).

If  $\tilde{\beta}$  approaches infinity, then for any bounded  $\tilde{\alpha}$ , (C.15) implies

$$\nabla^2 \omega_t^b = 0 ,$$

provided  $\omega_t^b$  and  $\lambda_b$  are bounded. Substitution of the boundary condition (C.27) leads to

$$\omega_t^b = \text{constant}. \quad (\text{D.9})$$

Combination of (D.9) and (C.25) yields

$$\nabla^2 \lambda_b = - \frac{\tilde{\omega}_t}{p_s - p_t} + \frac{\text{constant}}{p_s - p_t} . \quad (\text{D.10})$$

Furthermore, from (C.16) we have

$$\nabla^2 [(p_s - p_t) \nabla^2 \phi^{(0)}] = 0 , \quad (\text{D.11})$$

provided  $\lambda_b$  is bounded. The substitution of (C.23) into (D.11) leads to

$$\nabla^2 [(p_s - p_t) \nabla^2 \phi] = 0 ,$$

or

$$\nabla^2 \omega_t^\phi = 0 ,$$

by the use of (C.26). From the boundary condition (C.27), we have

$$\omega_t^\phi = \text{constant} , \quad (\text{D.12})$$

or

$$\nabla^2 \phi = \frac{\text{constant}}{p_s - p_t} ,$$

where  $d$  and  $a$  are bounded provided  $\tilde{\alpha}$  is bounded. Substitution of (D.9) and (D.12) into (C.24) leads to  $\omega_t = \text{constant}$ . Then,

applying the boundary condition (C.9), we get  $\omega_t = 0$ , identically. Therefore, Eq. (C.10) reduce to

$$\nabla^2 \lambda_1 = - \frac{\tilde{\omega}_t}{p_s - p_t} .$$

The above equation is exactly McGinley's formulation (1973).

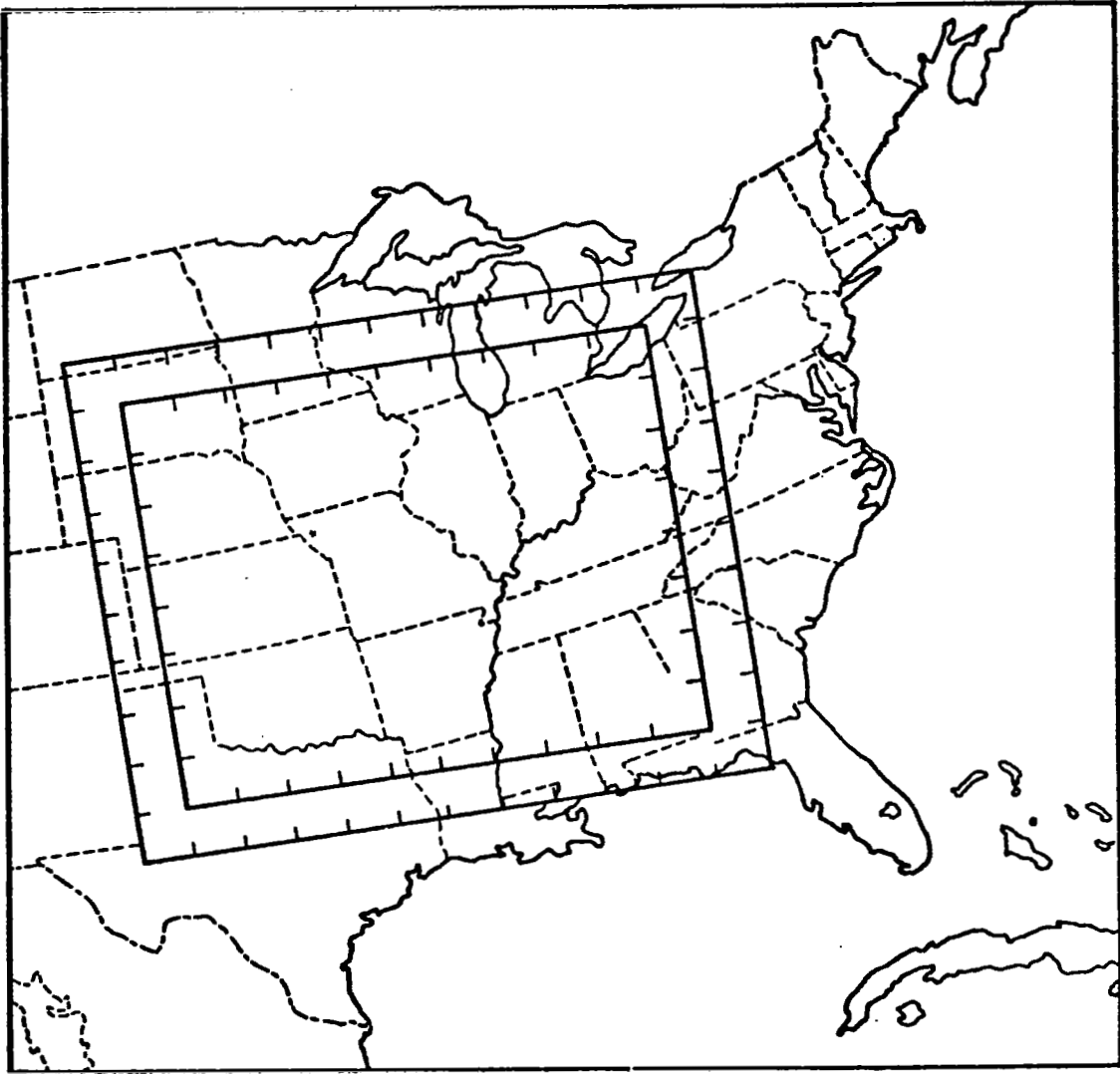


Fig. 1. Data grid and interior working grid.



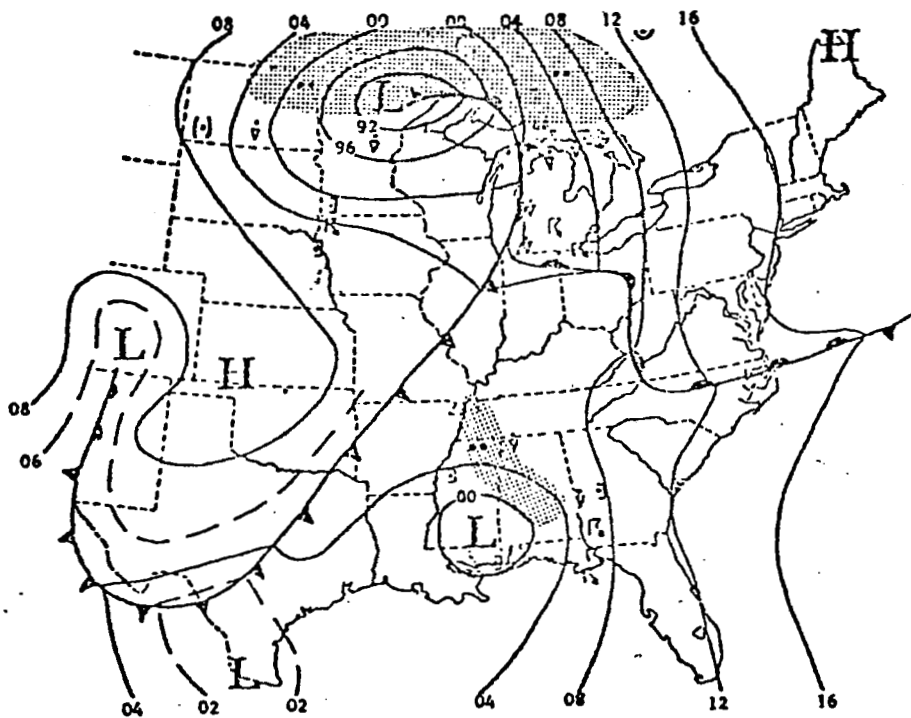


Fig. 2. Surface chart for 2100 GMT 11 May 1974. Isobars are drawn at 4 mb intervals.

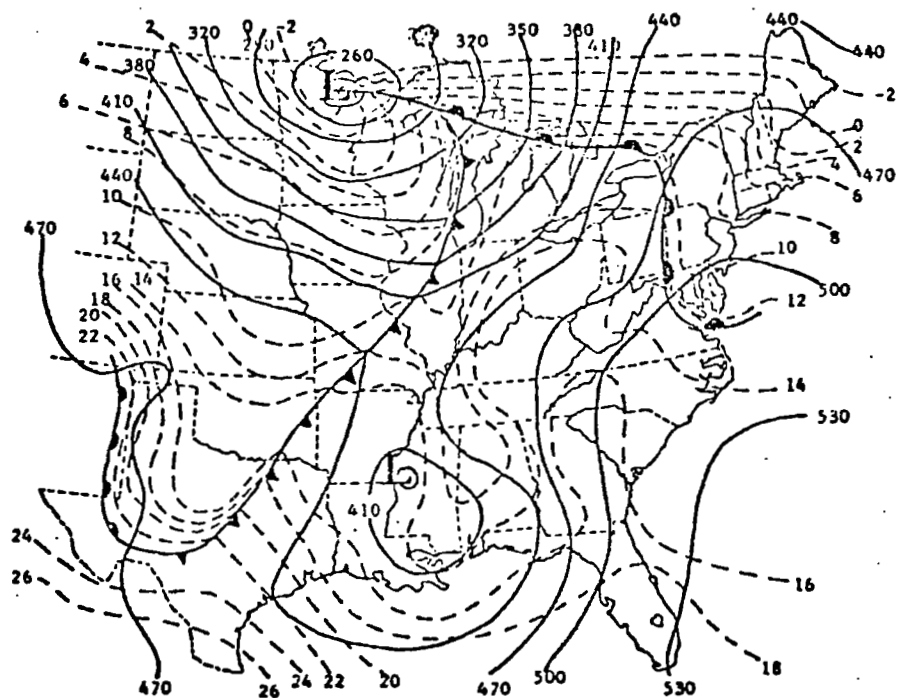


Fig. 3. 850 mb chart for 2100 GMT 11 May 1974. Height (solid) contours are drawn at 30 m intervals. Isotherms (dashed) are constructed at 2°C intervals.

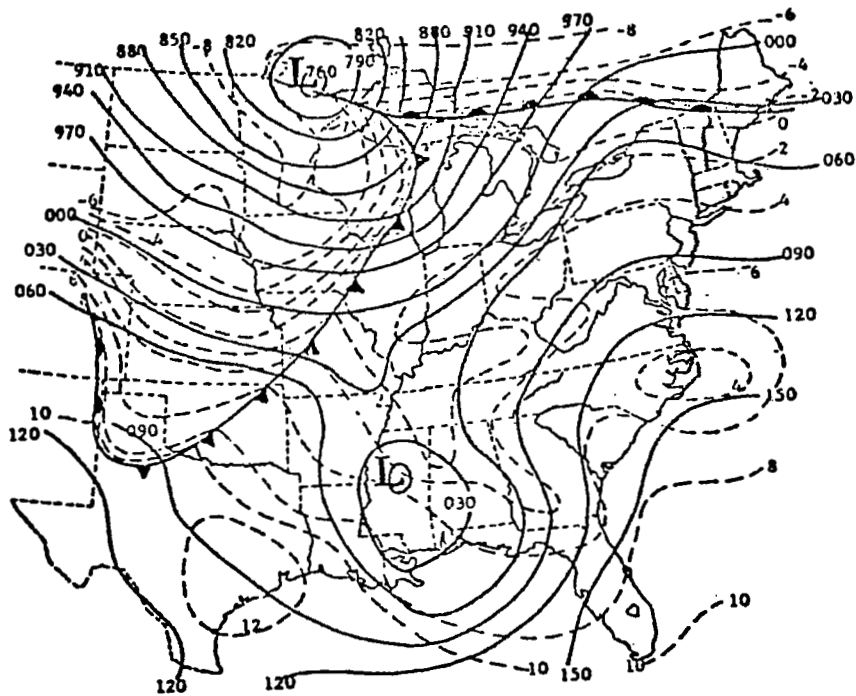


Fig. 4. Same as Fig. 3 except for 700 mb.

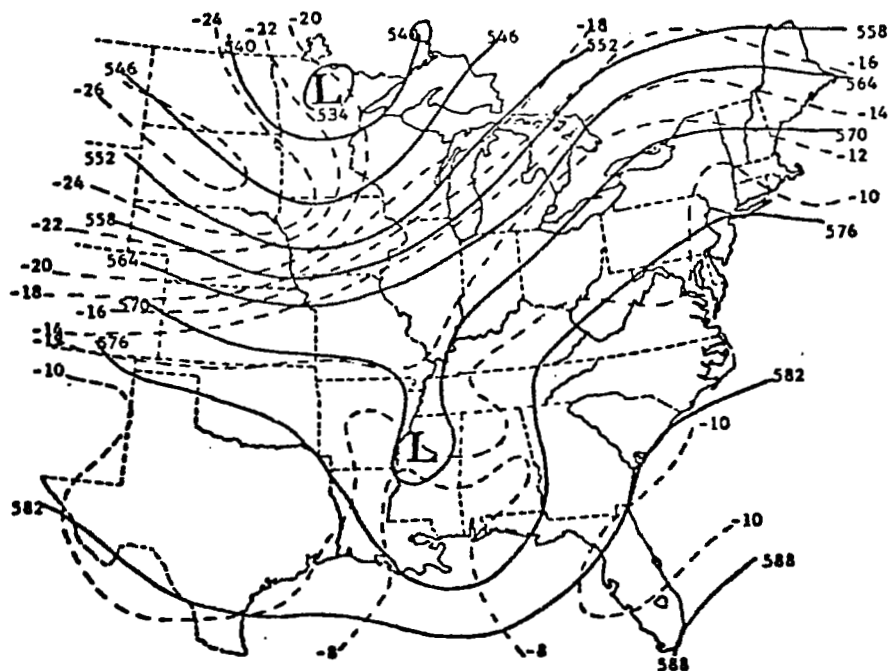


Fig. 5. Same as Fig. 3 except for 500 mb with contours drawn at 60 m intervals.

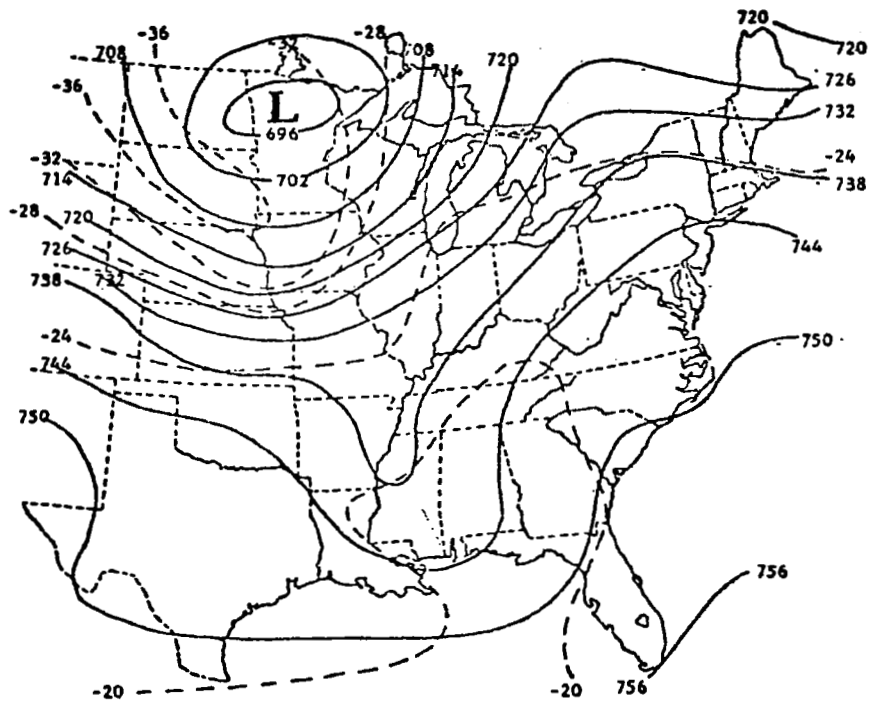


Fig. 6. Same as Fig. 3 except for 400 mb with contours drawn at 60 m intervals and isotherms constructed at 4°C intervals.

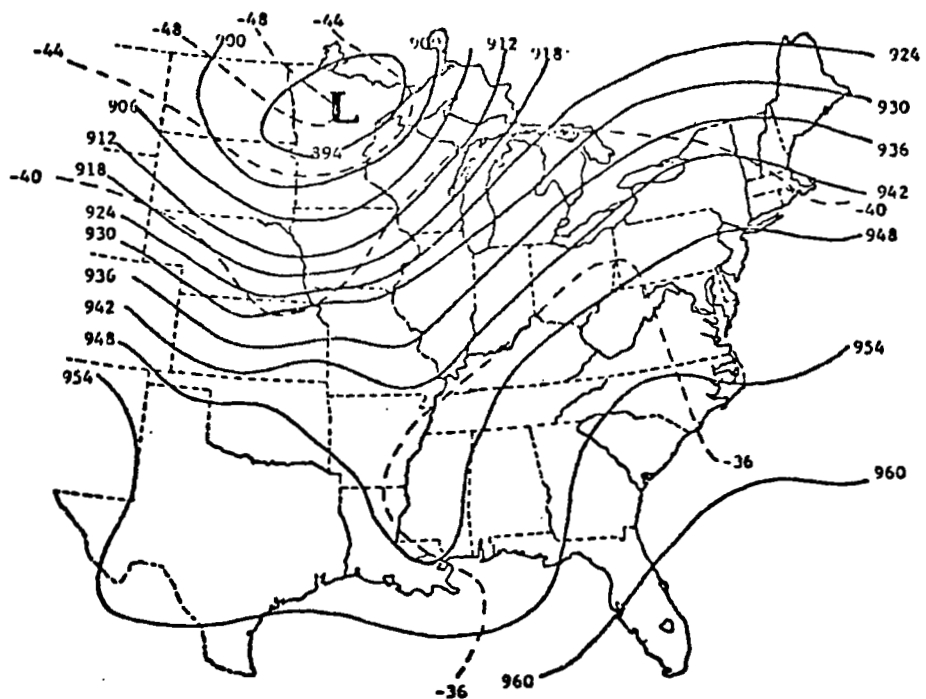


Fig. 7. Same as Fig. 3 except for 300 mb with contours drawn at 120 m intervals and isotherms constructed at 4°C intervals.



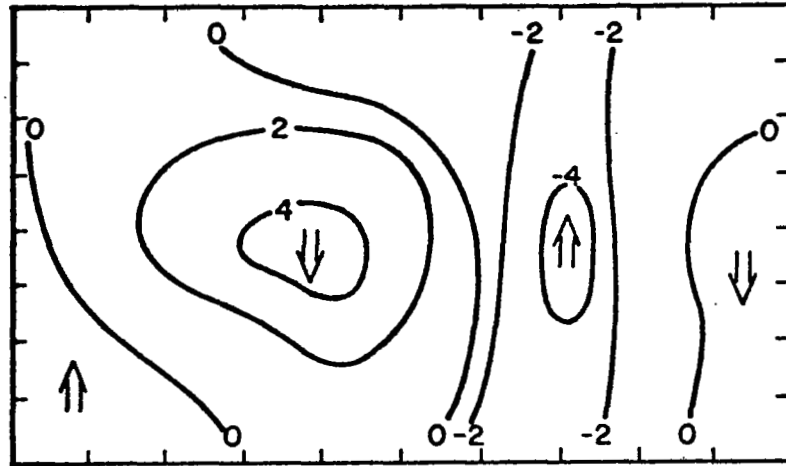


Fig. 10. Same as Fig. 9 except for 800 mb with isolines drawn at intervals of  $2 \mu\text{b sec}^{-1}$ .

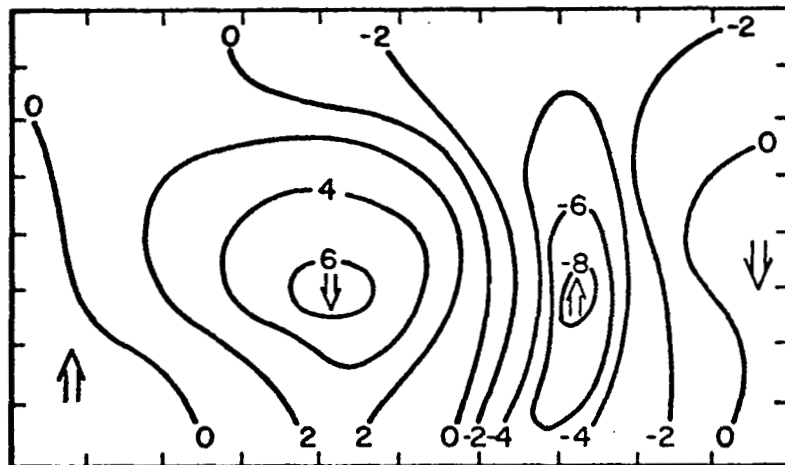


Fig. 11. Same as Fig. 9 except for 700 mb with isolines drawn at intervals of  $2 \mu\text{b sec}^{-1}$ .

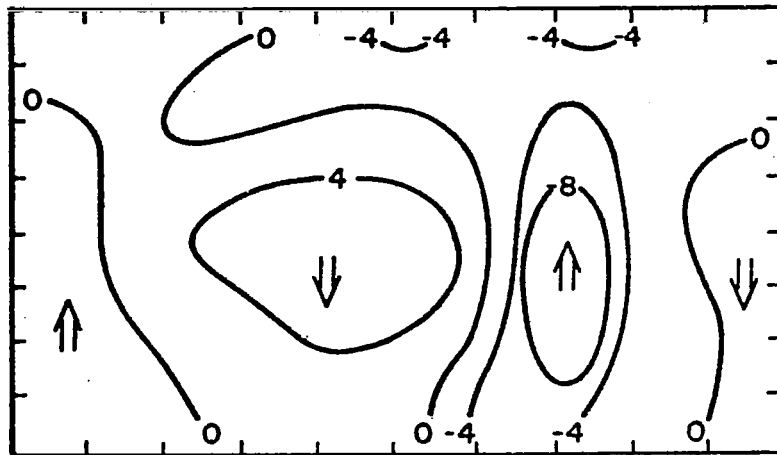


Fig. 12. Same as Fig. 9 except for 600 mb with isolines drawn at intervals of  $4 \mu\text{b sec}^{-1}$ .

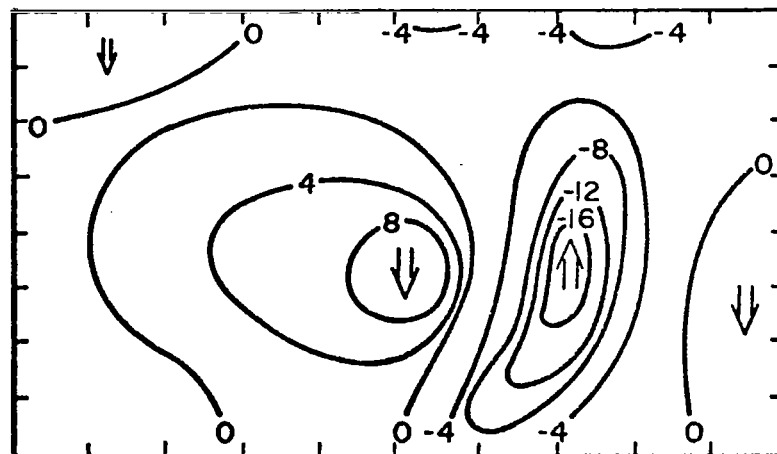


Fig. 13. Same as Fig. 12 except for 500 mb.

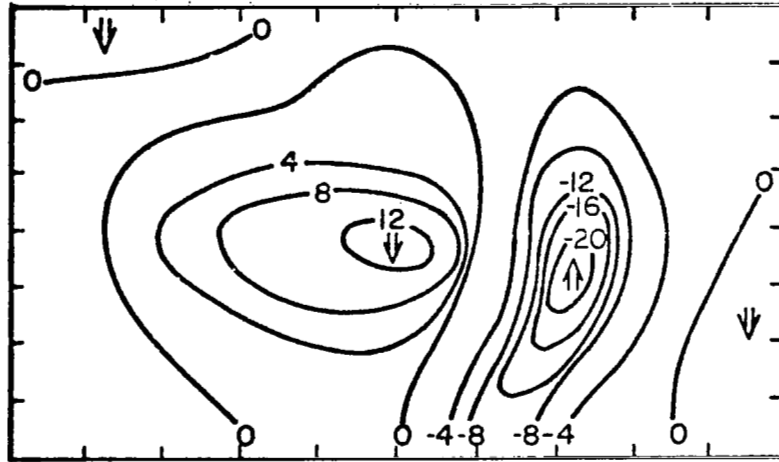


Fig. 14. Same as Fig. 12 except for 400 mb.

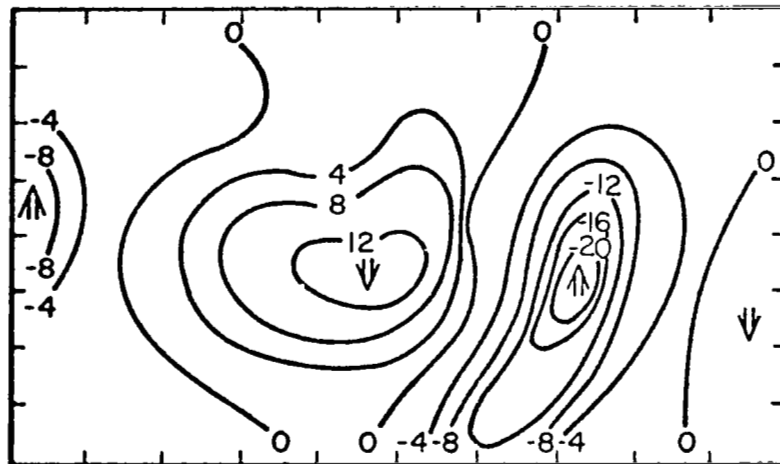


Fig. 15. Same as Fig. 12 except for 300 mb.

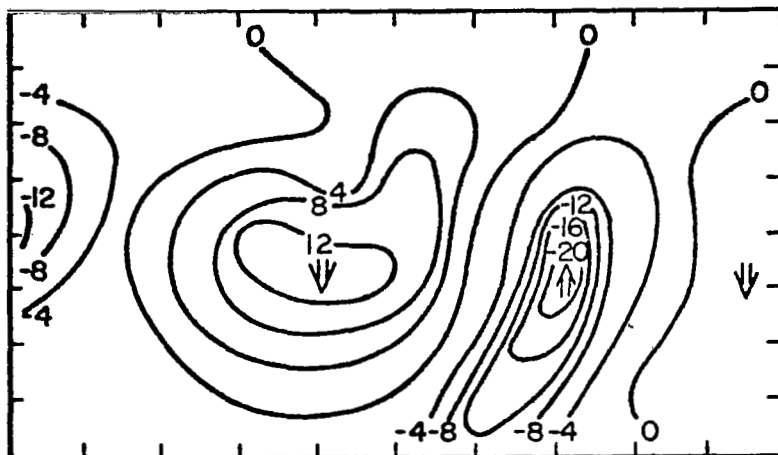


Fig. 16. Same as Fig. 12 except for 200 mb.

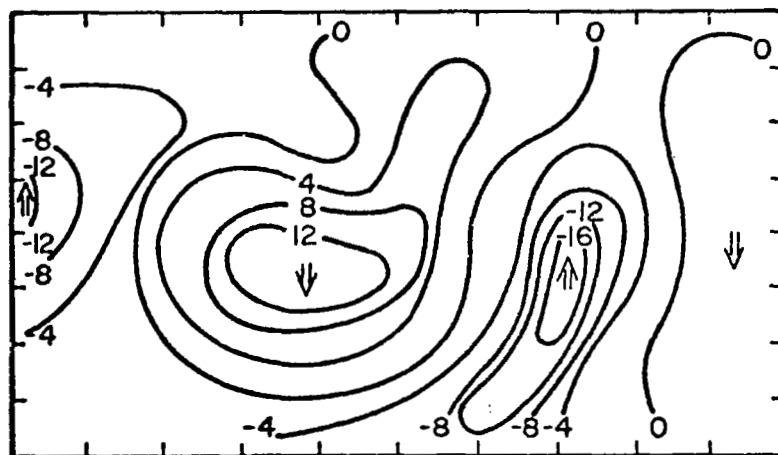


Fig. 17. Same as Fig. 12 except for 100 mb.



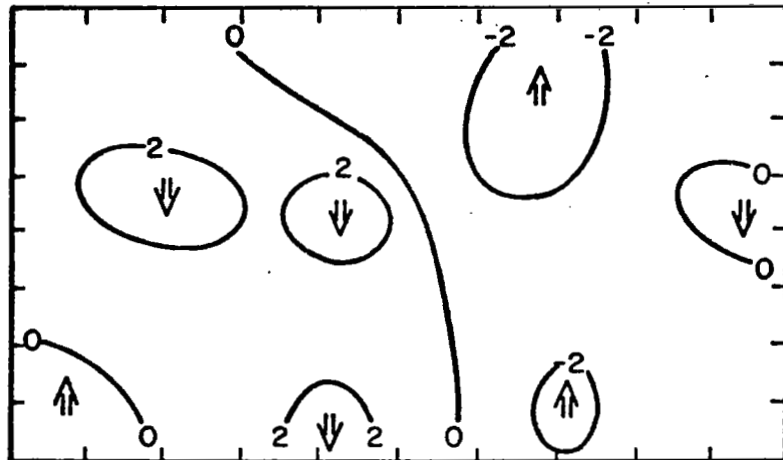


Fig. 18. Optimized vertical velocity,  $\omega$ , at 800 mb with isolines drawn at intervals of  $0.2 \mu\text{b sec}^{-1}$ .

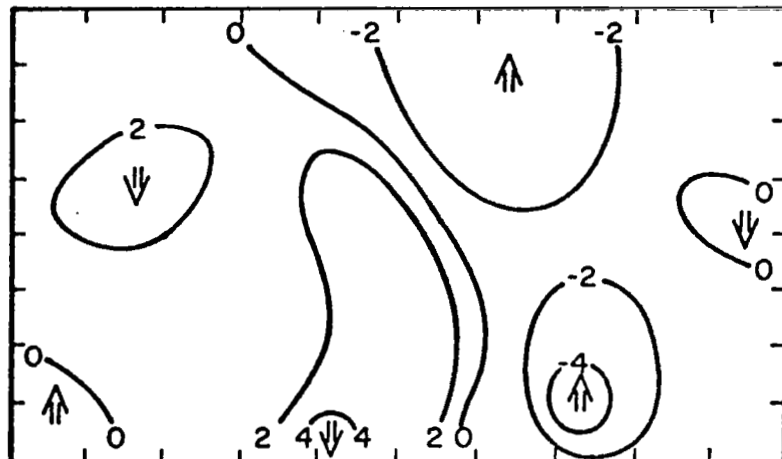


Fig. 19. Same as Fig. 18 except for 700 mb with isolines drawn at intervals of  $2 \mu\text{b sec}^{-1}$ .

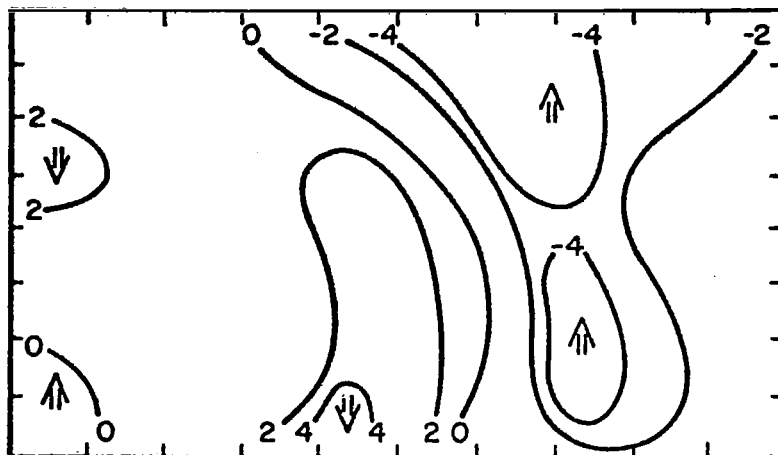


Fig. 20. Same as Fig. 19 except for 600 mb.

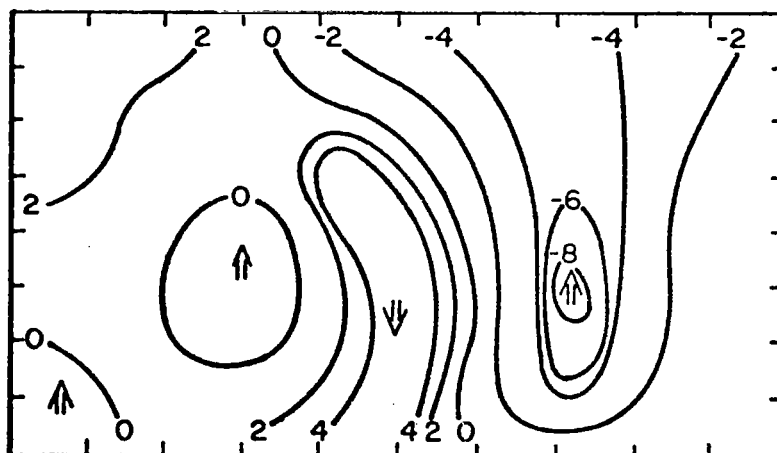


Fig. 21. Same as Fig. 19 except for 500 mb.

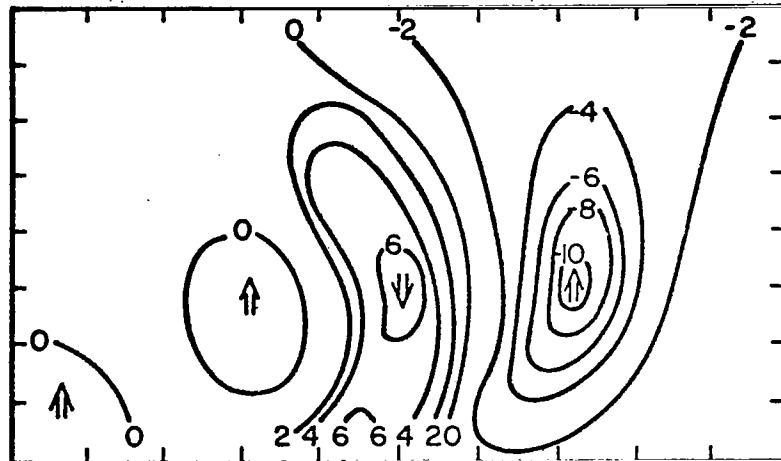


Fig. 22. Same as Fig. 19 except for 400 mb.

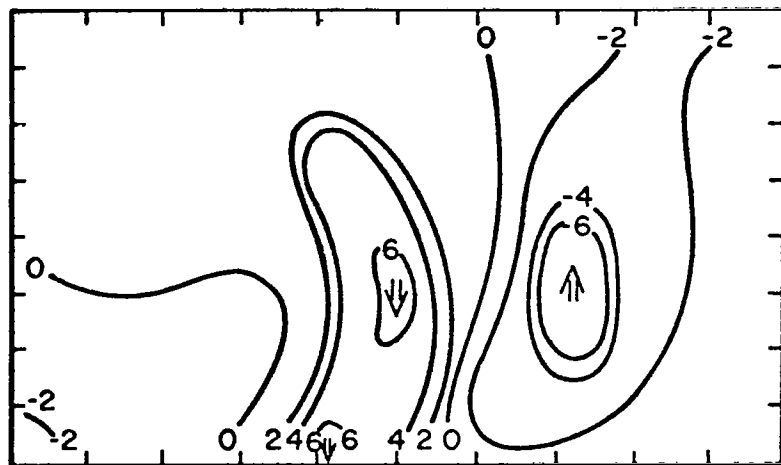


Fig. 23. Same as Fig. 19 except for 300 mb.

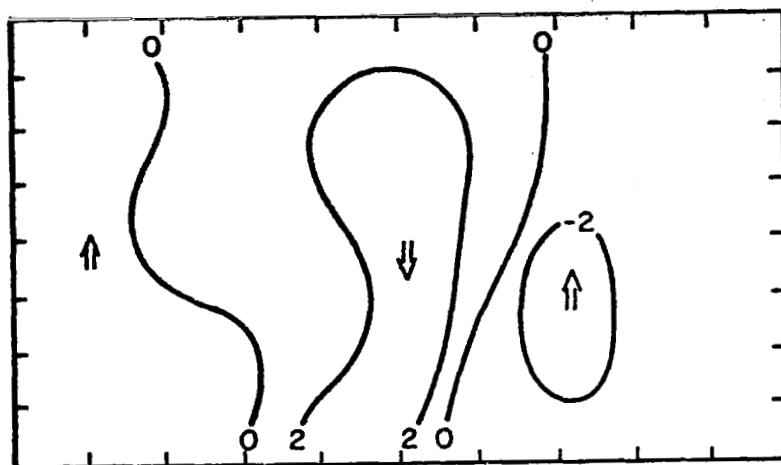


Fig. 24. Same as Fig. 19 except for 200 mb.

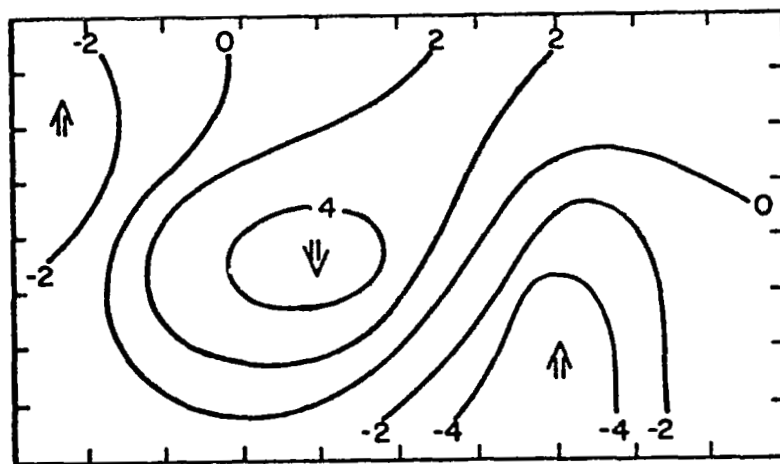


Fig. 25. Same as Fig. 18 except for 100 mb with isolines drawn at intervals of  $0.02 \mu\text{b sec}^{-1}$ .

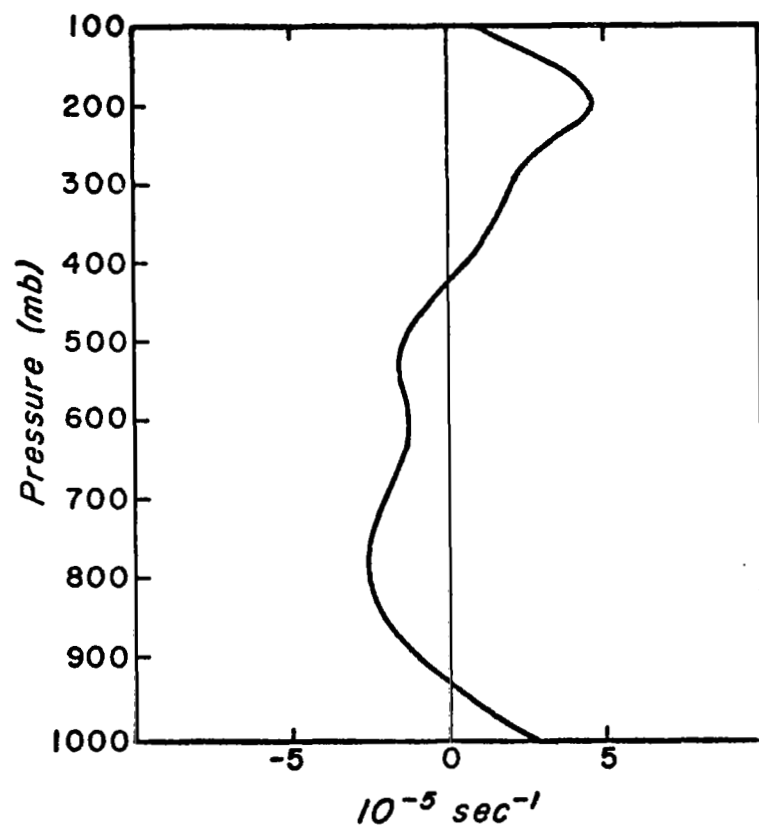


Fig. 26. Horizontal divergence at test point.

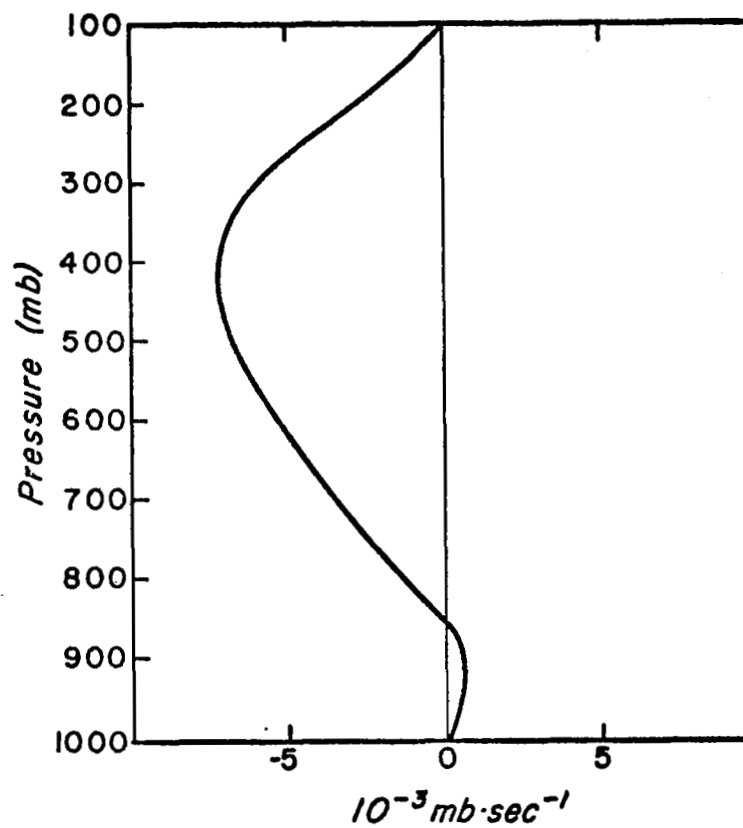


Fig. 27. Vertical velocity,  $\omega = \frac{dp}{dt}$ , at test point.

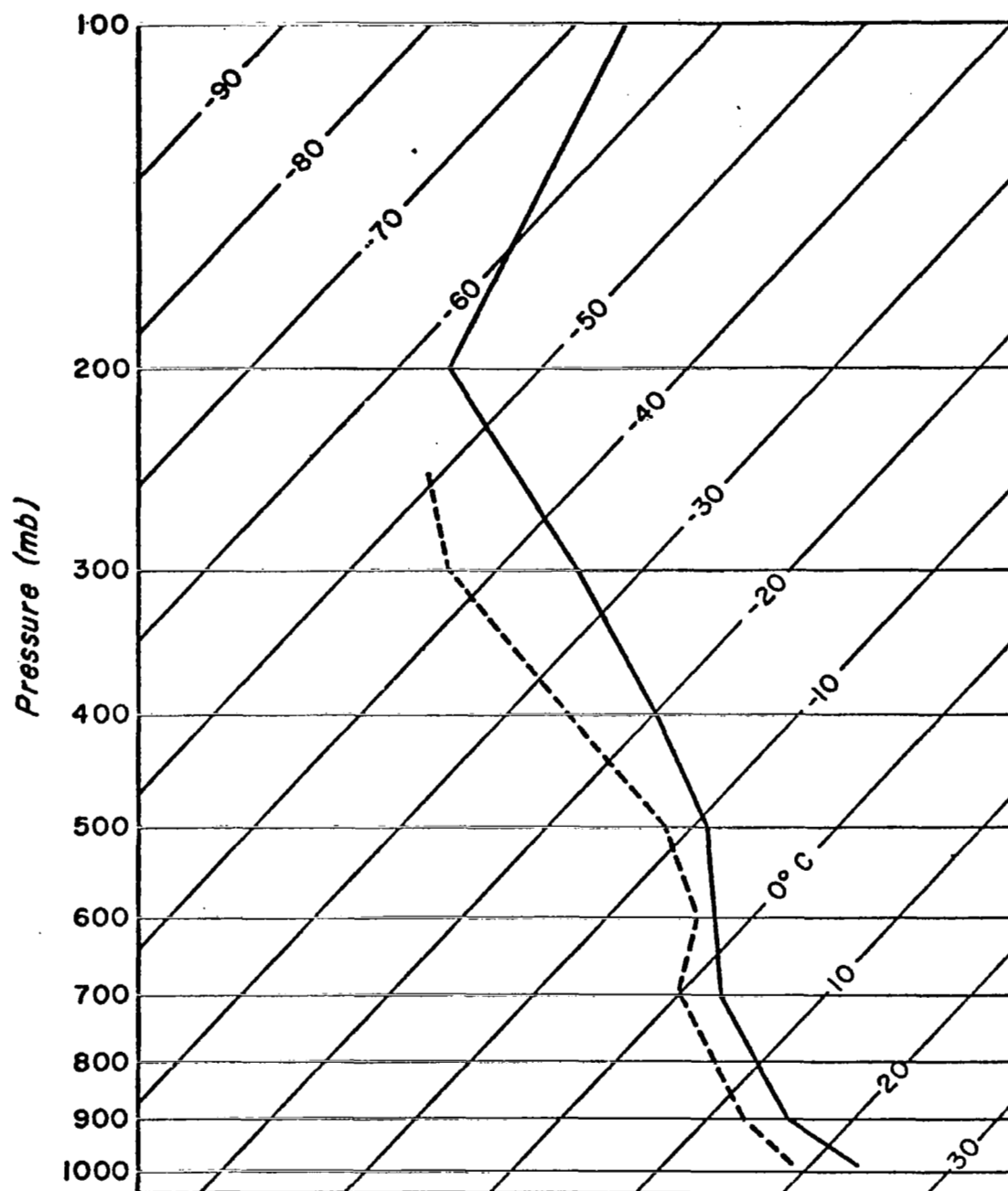


Fig. 28. Observed temperature and dew-point temperature at test point.

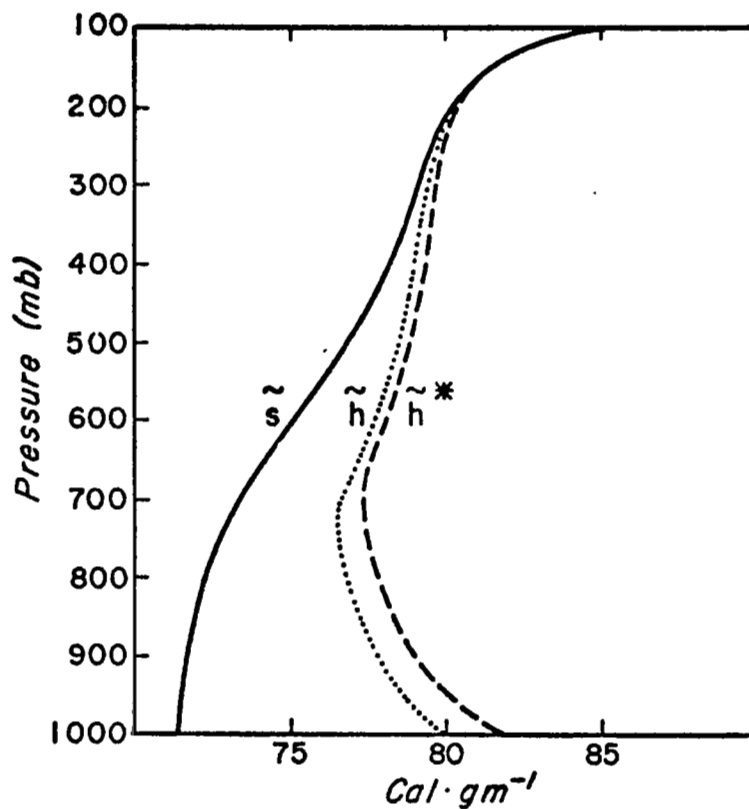


Fig. 29. The dry static energy,  $\tilde{s}$  (solid), moist static energy,  $\tilde{h}$  (dotted), and saturation moist static energy,  $\tilde{h}^*$  (dashed), of environment.

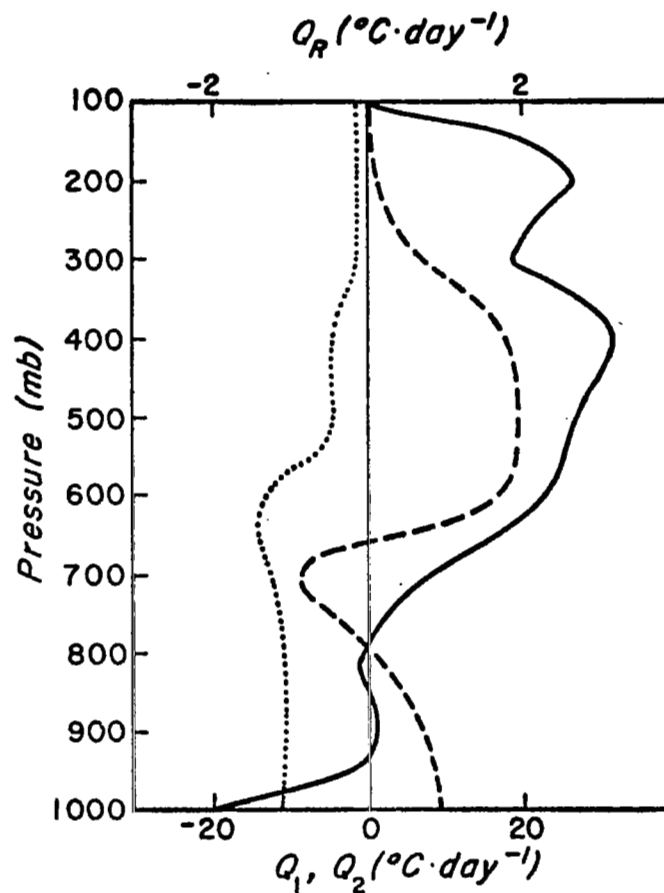


Fig. 30. The apparent heat source,  $Q_1$  (solid), the apparent moist sink,  $Q_2$  (dashed), and the radiational heating from Rodger's results (1967),  $Q_R$  (dotted).

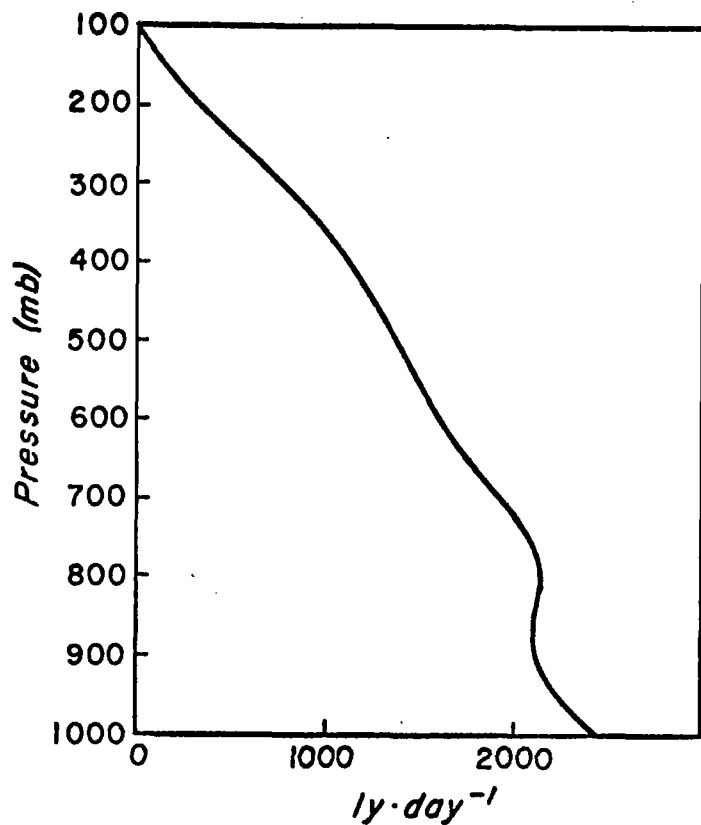


Fig. 31. The derived vertical eddy heat flux,  $Y$ .

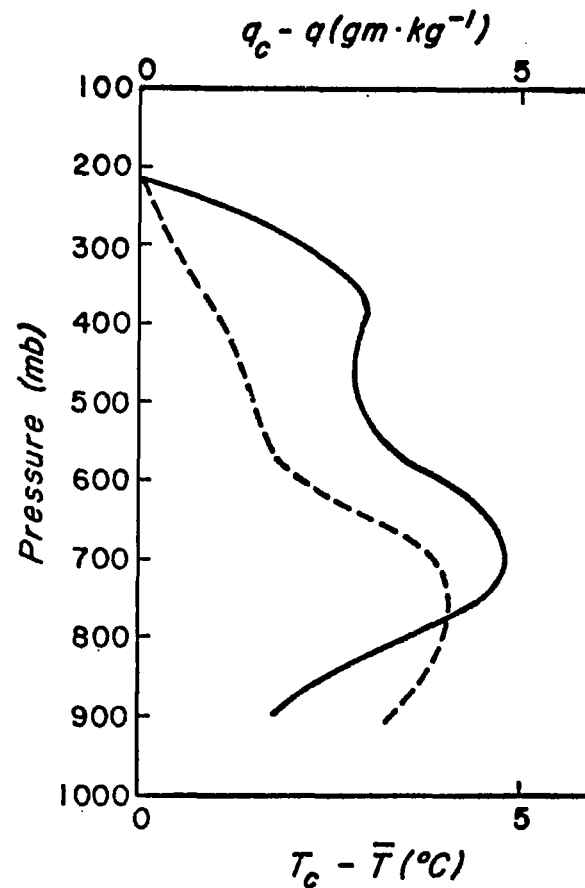


Fig. 32. The excess temperature,  $T_c - \bar{T}$  (solid), and the excess mixing ratio,  $q_c - \bar{q}$  (dashed), computed from the moist adiabat through the lifted condensation level representative of the surface layer.



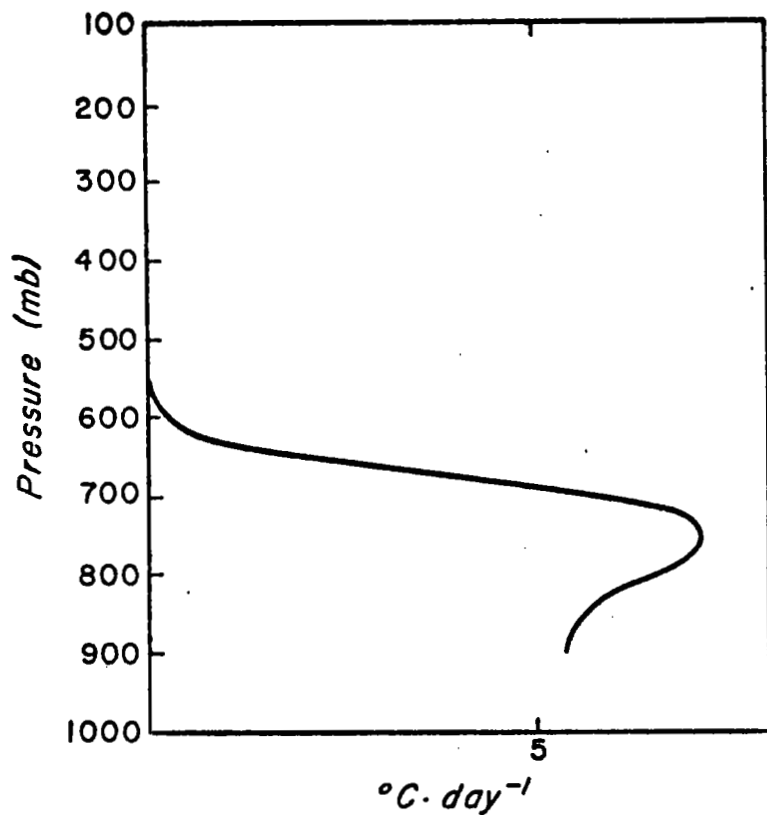


Fig. 33. Released latent heat, computed from large-scale budgets and Kuo's formulation.

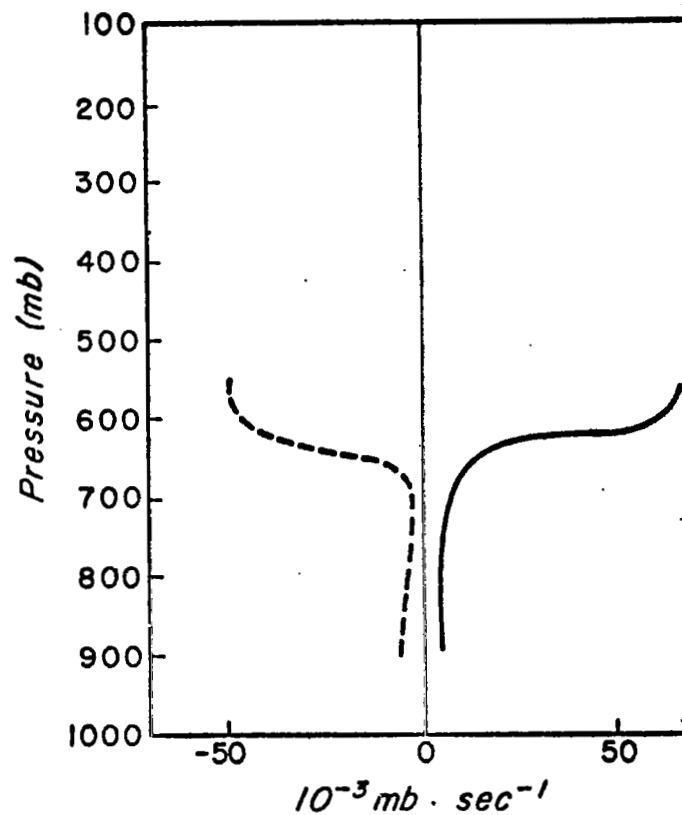


Fig. 34. Cumulative mass flux distribution within clouds,  $M_c$  (solid), and the corresponding environmental mass flux,  $M$  (dashed), computed from the large-scale budgets and Kuo's formulation of the latent heat released by subgrid-scale convection.

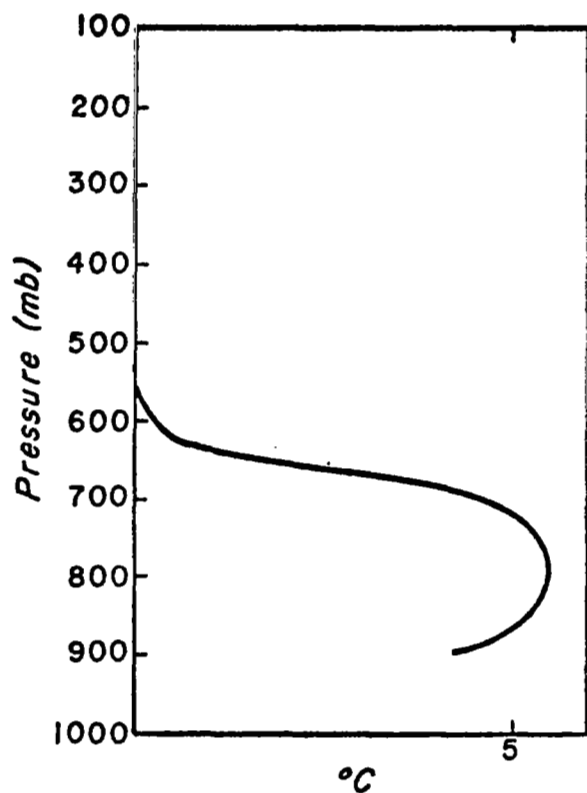


Fig. 35. The excess temperature,  $T_C - \bar{T}$ , computed from the large-scale budgets and Kuo's formulation of the latent heat released by subgrid-scale convection.

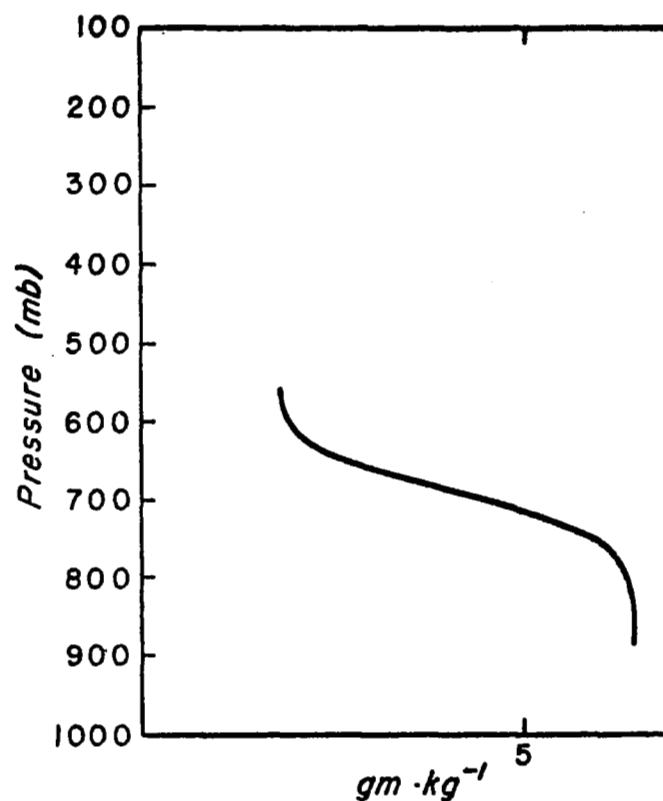


Fig. 36. The excess mixing ratio,  $q_C - \bar{q}$ , computed from the large-scale budgets and Kuo's formulation of the latent heat released by subgrid-scale convection.

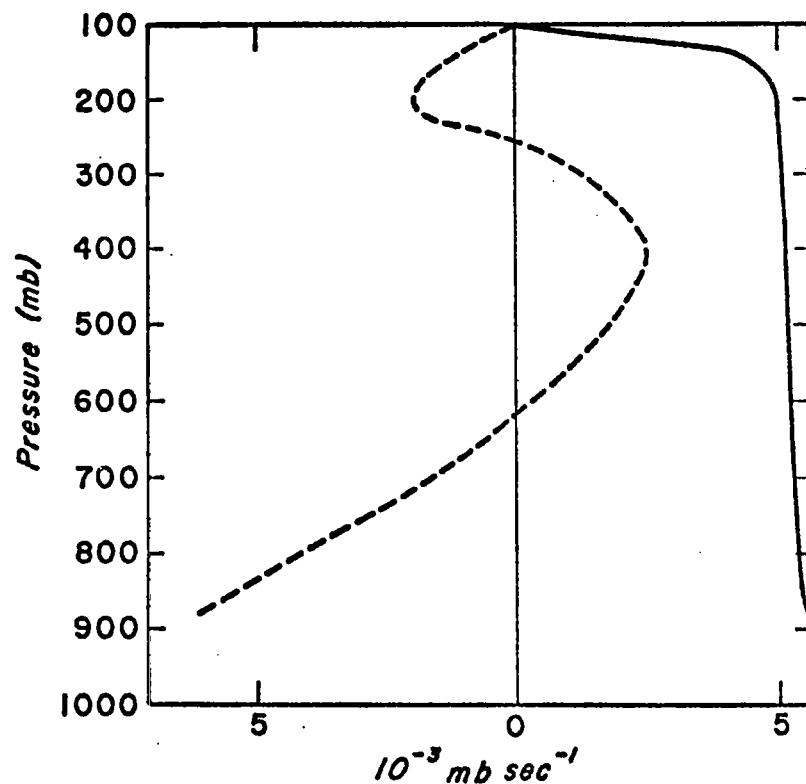


Fig. 37. Cumulative mass flux distribution within clouds,  $M_c$  (solid), and the corresponding environmental mass flux,  $M$  (dashed), computed from the large-scale budgets and the modified formulation of the latent heat released by subgrid-scale convection.

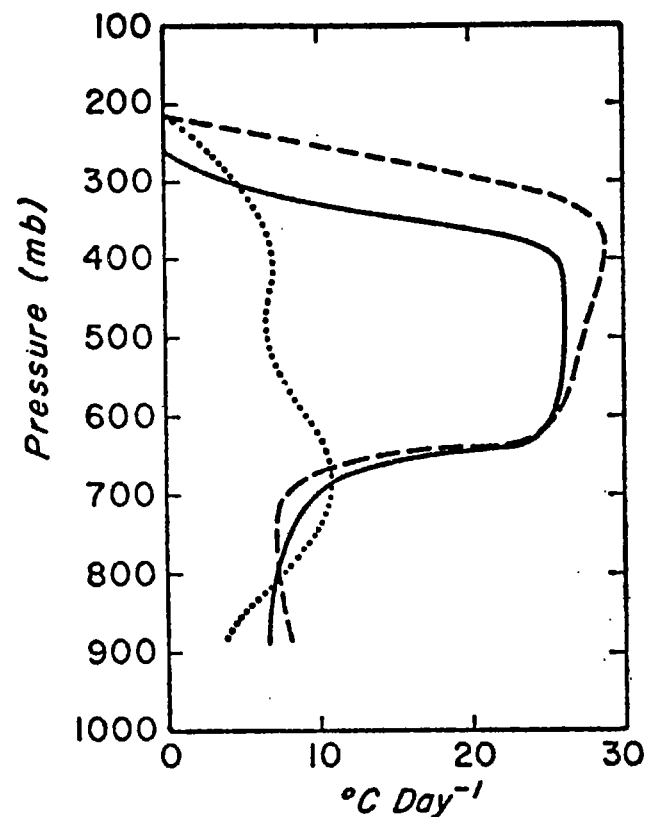


Fig. 38. The latent heat released by subgrid-scale convection, computed from (a) Kuo's scheme (dotted), (b) the modified scheme (dashed), and (c) the large-scale budgets and the modified formulation (solid).

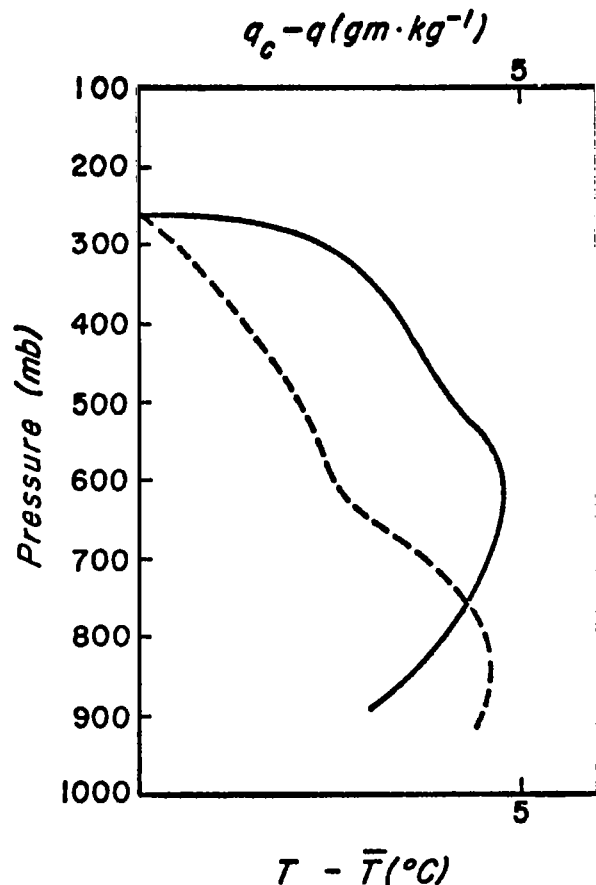


Fig. 39. The excess temperature,  $T_c - \bar{T}$  (solid), and the excess mixing ratio,  $q_c - \bar{q}$  (dashed), computed from the large-scale budgets and the modified formulation of latent heat released.

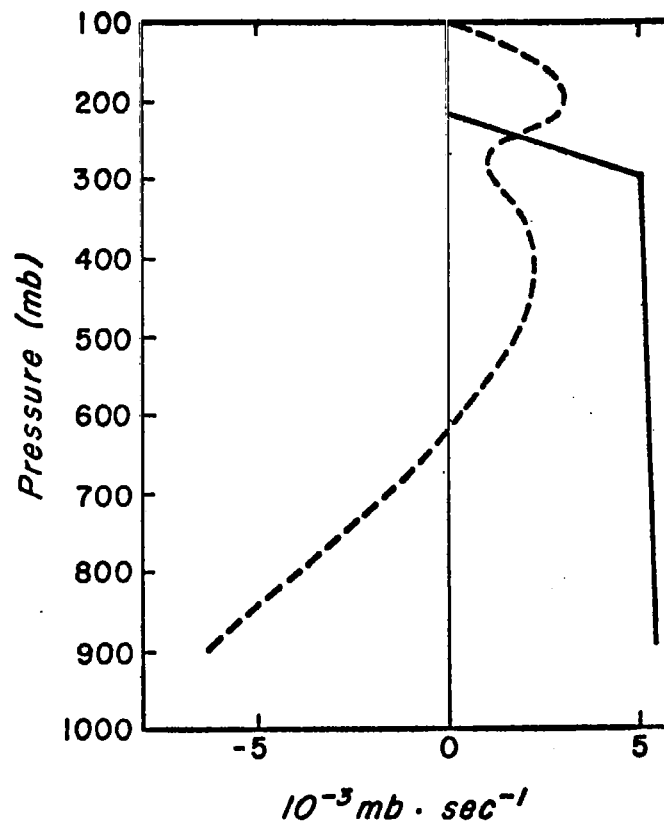


Fig. 40. Cumulative mass flux distribution within clouds,  $M_c$  (solid), and the corresponding environmental mass flux,  $\bar{M}$  (dashed), computed from the modified scheme.

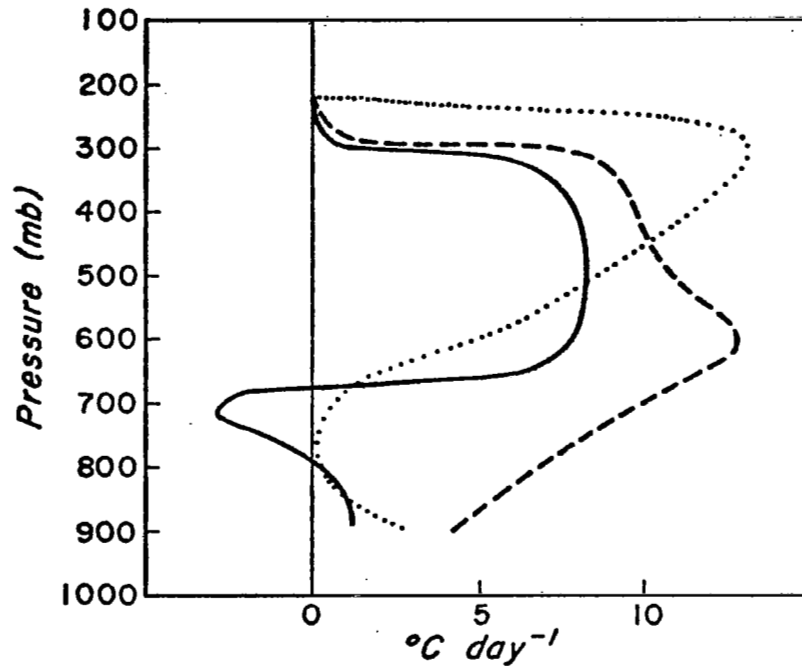


Fig. 41. The first (solid), the second (dashed), and the third (dotted) components of the expression for the latent heat released, computed from modified scheme.

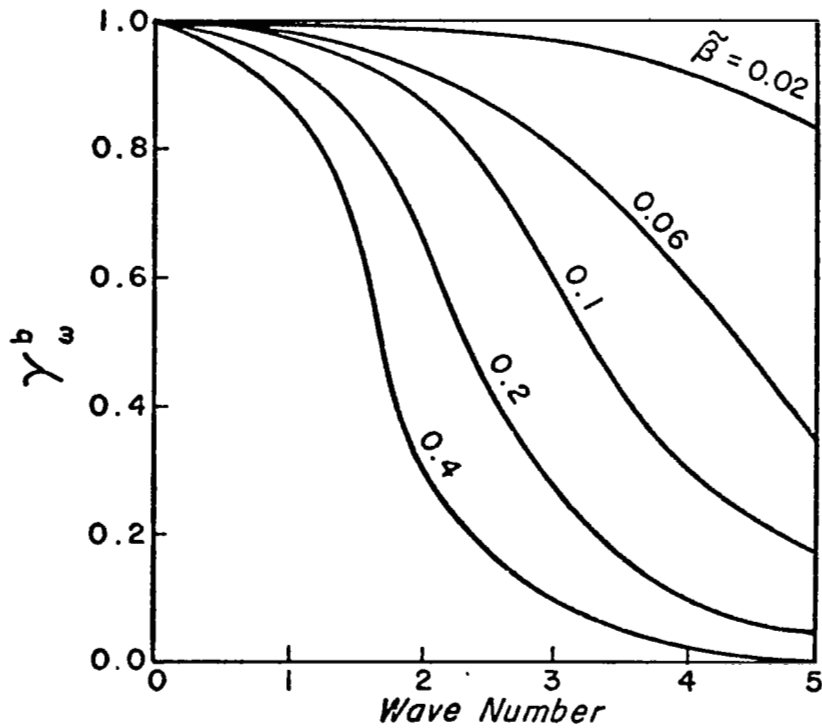


Fig. 42. The response function for  $\tilde{\alpha} = 0.1$ .

1. REPORT NO. NASA CR-2998		2. GOVERNMENT ACCESSION NO.		3. RECIPIENT'S CATALOG NO.	
4. TITLE AND SUBTITLE The Modification and Application of Kuo's Parameterization of Cumulus Convection in Middle Latitudes				5. REPORT DATE April 1978	
				6. PERFORMING ORGANIZATION CODE	
7. AUTHOR(S) Wen-Jey Liang				8. PERFORMING ORGANIZATION REPORT # M-249	
9. PERFORMING ORGANIZATION NAME AND ADDRESS  University of Oklahoma Norman, Oklahoma				10. WORK UNIT NO.	
				11. CONTRACT OR GRANT NO. NAS8-31333	
				13. TYPE OF REPORT & PERIOD COVERED  Contractor	
12. SPONSORING AGENCY NAME AND ADDRESS  National Aeronautics and Space Administration Washington, D. C. 20546				14. SPONSORING AGENCY CODE	
15. SUPPLEMENTARY NOTES  Prepared under the monitorship of the Atmospheric Sciences Division, Space Sciences Laboratory, NASA/George C. Marshall Space Flight Center					
16. ABSTRACT <p>In this study, the applicability of Kuo's parameterization of cumulus convection in the middle latitudes is examined, and a modification of his theory is developed. An evaluation of Kuo's scheme is performed to reveal physical insight into the involved mechanisms through a combination of the large-scale heat and moisture budgets and Kuo's formulation of the latent heat released. To improve upon the treatment of the interaction of deep convection with the environment, modifications consisting of considerations of the large-scale moisture supply and of the vertical transport of moisture and of dry static energy inside the cloud are made. Also, a two-layer cloud ensemble model is combined with the modified scheme. An examination of the modified scheme is performed by combining the large-scale heat and moisture budgets and the modified formulation of the latent heat released. The modified parameterization procedures are compared with Kuo's original scheme, and the results of tests of both schemes are discussed.</p> <p>For accurate computations of mass and moisture convergence, a variational optimization scheme is developed to analyze the wind field such that the integrated continuity equation and the global boundary condition are satisfied. Also, a low-pass filter is simultaneously incorporated in the optimization scheme to ensure that the filtered field satisfies the previously mentioned constraints.</p>					
17. KEY WORDS			18. DISTRIBUTION STATEMENT  Category 47		
19. SECURITY CLASSIF. (of this report)  Unclassified		20. SECURITY CLASSIF. (of this page)  Unclassified		22. PRICE  \$6.00	
				21. NO. OF PAGES  100	

\* For sale by the National Technical Information Service, Springfield, Virginia 22161